Wei Jia, Pan Cheng, Luping Ma, Shengqi Wang, Hua Qian, and Yuguo Li. (2022) Individual heterogeneity and airborne infection: Effect of non-uniform air distribution.*Building and Environment*.
doi:10.1016/j.buildenv.2022.109674

Individual heterogeneity and airborne infection: Effect of non-uniform air distribution

Wei Jia

Pan Cheng

Luping Ma

Shengqi Wang

Hua Qian

Yuguo Li

School of Energy and Environment, Southeast University, Nanjing, China

Corresponding author:Yuguo Li,Department of Mechanical Engineering, The University of Hong Kong, Pokfulam Road, Hong Kong, China
Email address: liyg@hku.hk

Submitted to *Building and Environment* July 12 2022

Accepted October 2022

Author Biographies

Wei Jia, PhD, is Postdoctoral Fellow in the Department of Mechanical Engineering at the University of Hong Kong. He obtained his PhD at the University of Hong Kong. His research interests are in airborne transmission mechanisms and engineering control for respiratory diseases in indoor environments.

Pan Cheng, PhD, is Postdoctoral Fellow in the Department of Mechanical Engineering at the University of Hong Kong. She obtained her PhD at the University of Hong Kong. Her research interests are in estimating quanta generation rate of respiratory viruses.

Luping Ma, MSc, was graduated from School of Energy and Environment at Southeast University, China.

Shengqi Wang, Phd, is a Lecturer at the School of Electric Power, Civil Engineering and Architecture, Shanxi University, China. Dr Wang's research focuses on healthy built environment including indoor air quality and microbial aerosols, data-driven environmental health analysis using machine learning methods, and coordinated control of wind–solar–thermal–energy storage systems.

Hua Qian, PhD, is Professor in the School of Energy and Environment at Southeast University, China. He obtained his PhD at the University of Hong Kong. His research interests are in indoor air quality, respiratory diseases transmission, computational fluid mechanics and energy saving in indoor environments.

Yuguo Li, PhD, is Chair Professor of Building Environment, Honorary Professor of School of Public Health, Associate Dean (Research) of Engineering. His research interests are in building environment engineering. His current research topics include city climate/environment, environment studies of infection and indoor environment.

Individual heterogeneity and airborne infection: Effect of non-uniform air distribution

Abstract

The classical Wells–Riley equation assumes homogeneity of susceptible individuals and environments to airborne exposure. However, individual susceptibility to infection is mostly heterogeneous, and exposure variability could arise from differences in inhalation rate, spatiotemporal non-uniformity of infectious aerosol concentrations, and the exposure trajectory and time. Non-uniform air distribution results in spatial non-uniformity of infectious aerosol concentrations. The non-uniformity effect is essentially a problem of individual infection probability. Here, we derived a general dose-response equation and a heterogeneous Wells–Riley equation accounting for individual variability in infection probability. The heterogeneous Wells-Riley equation shows the potential of the zone air distribution effectiveness to consider spatial non-uniformity under steady-state conditions. An existing quanta generation rate formula was theoretically justified. The new equation was then applied to a restaurant reporting an outbreak of coronavirus disease 2019, with spatial and/or temporal heterogeneity of infectious aerosol concentrations. Our results show the need to include spatial non-uniformity in outbreak investigations. A hypothetical two-zone setup was used to demonstrate how the inter-zonal distribution of clean air and the inter-zonal exchange flow affect airborne infections. An infector in a poorly diluted zone with the greatest number of susceptible individuals would result in the least secondary infections, whereas an infector in a well-ventilated zone with few susceptible individuals would result in the least secondary infections.

(216 words)

Key words

Effective dilution air, intake fraction time, Poisson-binomial distribution, Wells–Riley equation, SARS-CoV-2 transmission

1.Introduction

Airborne transmission has been accepted as a major route for the spread of severe acute respiratory syndrome coronavirus 2 (SARS-CoV-2) and is suspected to be a major route of transmission for most other respiratory infections (Tang et al., 2022). Unlike investigations of infections originating from food and water (WHO, 2003), quantitative microbial risk assessments (QMRA) have not been widely used for airborne infection investigations (Haas, 2021). The Wells–Riley equation (Riley et al., 1978) has traditionally been used to model the airborne transmission of infectious diseases (Gammaitoni and Nucci, 1997; Rudnick and Milton, 2003). Parhizkar et al. (2021) proposed a QMRA-based dose-response model of the airborne transmission of SARS-CoV-2 that accounts for particle emission dynamics, particle deposition to indoor surfaces, ventilation rate, and filtration.

These existing models of airborne transmission assume individual homogeneity in susceptibility and exposure. However, significant heterogeneity in susceptibility exists for some respiratory infections, e.g., SARS-CoV-2, due to different levels of immunity (Moghadas et al., 2021) and contact. The Wells–Riley equation and dose-response models have traditionally been considered to be two different modelling categories (Sze To and Chao, 2010). The relationship between the two models is discussed later in this paper. The respiratory deposition of aerosols differs from the ingestion of pathogens contained in food or water due to variations in deposition site and efficiency (Sze To and Chao, 2010; Parhizkar et al., 2021). As one major intervention method, ventilation dilutes infectious aerosols in an occupied space, but its effectiveness differs locally as the concentration of infectious aerosols may be non-uniform within a space. Imagine the trajectory of a susceptible individual who may walk through a space and stay at different locations. Each susceptible individual has a unique exposure trajectory. Sze To and Chao (2010) considered the spatial distribution of aerosols as one of the most important factors in the risk assessment of respiratory infections. Sze To et al. (2008) proposed an exposure assessment model using spatial distribution of expiratory aerosols and the viability of airborne viruses. To model non-uniform distributions, Qian et al. (2009) implemented an approach using computational fluid dynamics (CFD) and the infectious quantum concept.

During the coronavirus disease 2019 (COVID-19) pandemic, an outbreak in a restaurant in Guangzhou was shown to likely occur via airborne transmission (Li et al., 2021). Reconstruction of the airflow at the time of exposure in the restaurant using CFD revealed a relatively stable air recirculation bubble in the Table ABC zone, where all secondary infections occurred (Figure 3 in Li et al., 2021). One major question was asked by several experts when the project team presented the study, i.e., would there have been fewer secondary infections if there was better mixing between the Table ABC zone and non-ABC zone? One inherent factor makes it difficult to answer this question. The 89 patrons in the restaurant arrived at and departed from the restaurant at different times. Therefore, there was significant heterogeneity in individual levels of exposure. It is difficult to estimate the number of secondary infections using the traditional Wells-Riley equation when there are significant differences in the probability of infection between individuals. Additionally, heterogeneity in individual exposure levels also occurred due to the non-uniform distribution of infectious aerosols in this restaurant. Similar levels of spatiotemporal non-uniformity of infectious aerosols and individual heterogeneity exist in other public spaces.

Air distribution is not difficult to analyse, but the existing Wells–Riley equation cannot be used for non-uniform conditions. Three-dimensional air distribution has been modelled since the 1980s, when CFD simulations were first applied to air distribution analysis (Nielsen et al., 1978). At any spatial point in a space, we can now estimate the local age of the air (i.e., the time since the first arrival of the air in a specific place), the remaining time a contaminant will be present (before being removed from the space), and the local ventilation index (the ratio of the local concentration and the concentration at exhaust) (Etheridge and Sandberg, 1996). The existing ventilation standard (ASHRAE 62.1, 2019) uses the ‘zone air distribution effectiveness’ measure, E_z, which measures ‘how effectively the zone air distribution uses its supply air to maintain the acceptable air quality in the breathing zone’. The

required minimum ventilation is scaled according to the E_z value. In a room with poor air distribution, a larger ventilation rate is needed. The question remains regarding how poor air distribution affects infection risk.

The key to studying the non-uniformity effect on airborne infections lies in developing a risk assessment model that considers the individual probability of infection. In addition to non-uniformity, individuality of infection risk may also arise from different exposure times, even under uniform conditions and/or at individual susceptibility levels. Integrating uncertainty and interindividual variability into risk assessment has been well studied in food and water microbiology (Bogen and Spear, 1987).

Here, we extended a QMRA-based dose-response model used in food and water microbiology for application to airborne transmission risk assessment. This resulted in a new Wells–Riley equation for use in multiple heterogeneous conditions, e.g., non-uniform and temporally varying air distribution. Our key idea was to follow the exposure trajectory of a susceptible individual in a room and estimate *individual* inhalation probabilities of a virus particle (or virion) in a space. The individual probability of infection was then estimated using the single-hit model reported by Haas (1983). The population infection risk in the space was estimated using a Poisson-binomial distribution, as reported by Bogen and Spear (1987) and Nicas (1996). The relationship between this general dose-response model of airborne infection and the Wells–Riley equation was naturally established. A new heterogeneous Wells–Riley equation was then used to analyse the aforementioned restaurant outbreak and a hypothetical outbreak in a two-zone restaurant setting.

2.Methodologies

2.1 Individual inhalation probability of a virion in room air

The inhalation probability of an airborne virion by individual i is fundamental to airborne infection risk analysis. However, this probability has not been analysed in previous studies. Each inhalation event differs. An individual may be at different locations in a room and have different inhalation rates due to differences in physical activity, respiratory activity, and posture. The concentration of aerosols or virions also varies with both space and time.

Consider a room with an air volume of V (m^3), N_σ susceptible individuals, and N_I infectors. For respiratory infections, two populations are involved: virus particles or virions and susceptible individuals. Each virion in the room may be inhaled by a susceptible individual and produce an infection.

Each point in space was defined as $\boldsymbol{x}(x, y, z)$. The trajectory of an individual was denoted as $\vec{x}(t)$ at moment t. The airborne virion concentration, $c_V(\boldsymbol{x}, t)$, varied both spatially and temporally (Figure 1A). CFD predictions may be used to determine $c_V(\vec{\boldsymbol{x}}, t)$ (Qian et al., 2009), and/or fine spatial- or temporal-resolution measurements may become possible in the future.

<Figure 1> Model of an enclosed space, individuals, and their trajectories. (A) Breathing zone in a room with one infector (in red) who caused an outbreak of a

respiratory infection amongst 19 susceptible individuals, with three infected (in yellow) and 16 not infected. (B) The spatial trajectory, $\vec{\boldsymbol{x}}_i(t)$, of individual i who arrives at time $t_{1,i}$ and departs at time $t_{2,i}$. The sphere symbols show the locations where individual i spends some time. (C) The concept of the space–time prism for defining the trajectory, $\vec{\boldsymbol{x}}_i(t)$, of individual i in the space.(For interpretation of the references to colour in this figure legend, the reader is referred to the Web version of this article.)

We focused on a susceptible individual, i. The inhalation exposure of individual i, $n_{in,i}$, is proportional to the inhalation flow rate, $q_{in,i}(t)$, and thus, $q_{in,i}$ may change with time along individual i's trajectory, $\vec{\boldsymbol{x}}_i(t)$. Individual i arrives in the space at time $t_{1,i}$ and departs at time $t_{2,i}$ (Figure 1B), and $c_V(\vec{\boldsymbol{x}}_i(t))$ is the virion concentration along trajectory $\vec{\boldsymbol{x}}_i(t)$. Strictly speaking, $c_V(\vec{\boldsymbol{x}}_i(t))$ is the virion concentration in the inhaled air volume, $q_{in,i}(t)dt$. Our notion of trajectory $\vec{\boldsymbol{x}}_i(t)$ may be seen as an application of the space–time prism (Miller, 1991, and Figure 1C) in indoor spaces.

The number of virions inhaled by individual i in space can be represented by: $n_{in,i} = \int_{t_{1,i}}^{t_{2,i}} q_{in,i}(t) c_V(\vec{\boldsymbol{x}}_i(t))\, dt$.

The average number of virions in a space during the entire stay period of individual i can be calculated as:

$$n_{v,i} = \frac{\int_{t_{1,i}}^{t_{2,i}} \int_0^V c_V(\boldsymbol{x},t) dV\, dt}{t_{2,i} - t_{1,i}},$$

where $c_V(\boldsymbol{x}, t)$ is the virion concentration at location $\boldsymbol{x}$ and time t. Note the difference between $c_V(\boldsymbol{x}, t)$ and $c_V(\vec{\boldsymbol{x}}_i(t))$, which represent all spatial locations $\boldsymbol{x}$ in space and only those spatial points, $\vec{\boldsymbol{x}}_i$, along the trajectory of individual i, respectively.

For any virion in space, its inhalation probability by individual i during the whole exposure period becomes

$$p_{in,i} = \frac{n_{in,i}}{n_{v,i}}. \qquad (1)$$

Equation (1) is important and fundamental. When it is in a steady state and $c_V(\vec{\boldsymbol{x}})$ is uniformly distributed, $p_{in,i} = \frac{q_{in,i} c_V \Delta t_i}{V c_V} = \frac{q_{in,i} \Delta t_i}{V}$. The new Equation (1) paves the way to estimate the individual infection probability due to inhalation exposure and the number of secondary infections in a space.

2.2 Probability of infection of an individual

The probability that a virion is not inhaled by individual i becomes $1 - p_{in,i} = 1 - \frac{n_{in,i}}{n_{v,i}}$.

The probability that j virions are inhaled by individual i follows a binomial distribution, as indicated in Equation (2).

$$p_{(j)} = \Pr(X = j | n_{v,i}, p_{in,i}) = \frac{n_{v,i}!}{j!(n_{v,i}-j)!} {p_{in,i}}^{j} (1 - p_{in,i})^{n_{v,i}-j} \qquad (2)$$

Individuals vary in their level of immunity and other risk factors for respiratory infections. The survival and infection probabilities of the virions inhaled by an individual may also be 'individual'. We used a dose-response parameter, r_i, for susceptible individual i to denote such individual variability. The survival of a virion from its release to infection was assumed to be independent. By definition, $r_i = 1$ when the infectious quantum is used as the infectious unit (Sze To and Chao, 2010).

Using the single-hit model approach described by Haas (1983), we further obtained the infection probability of individual i (the details are listed in Supplementary Information S2). The probability that one or more of the $n_{v,i}$ virions are inhaled by susceptible individual i, survive, and lead to infection based on the single-hit theory becomes

$$p_i(d_i) = 1 - e^{-r_i d_i}, \qquad (3)$$

where the dose, $d_i = n_{v,i} p_{in,i} = \int_{t_{1,i}}^{t_{2,i}} q_{in,i}(t) c_V(\vec{x}_i(t)) dt$, with the individual-based dose-response parameter r_i. If all parameters are available, the probability of infection, p_i, can be obtained for every individual ($i = 1,2,\dots,N_\sigma$).

2.3 Expected average number of infected individuals

We estimated the expected number of infected individuals (N_ι) amongst N_σ susceptible individuals in a space. This estimation is equivalent to performing N_σ independent experiments, i.e., Bernoulli trials, with the i^{th} experiment (individual i) having a probability of success (infected), p_i, or a probability of failure (not infected), $(1 - p_i)$. The probability that k susceptible individuals ($k \leq N_\sigma$) are infected can be written as a Poisson-binomial distribution (Bogen and Spear, 1987; Nicas, 1996). Following the method detailed in Supplementary Information S3, we obtain the average infection probability in the space

$$\frac{N_\iota}{N_\sigma} = \bar{p}_i = 1 - \frac{1}{N_\sigma} \sum_{i=1}^{N_\sigma} (e^{-r_i d_i}), \qquad (4)$$

where $\bar{p}_i = \frac{\sum_{i=1}^{N_\sigma} p_i}{N_\sigma}$ is the average infection probability of N_σ susceptible individuals. The Poisson-binomial distribution also allows estimation of the probability that any k susceptible individuals ($k \leq N_\sigma$) get infected.

The dose-response model (Equation 4) predicts the expected number of secondary infections (N_ι), with each susceptible individual having their own probability of infection. In this new model, the exposure dose, d_i, and the dose-response parameter, r_i, may differ for each susceptible individual. In theory, when the ventilation rate or the *clean air flow rate* is given for a group of susceptible individuals and infectors, along with their detailed trajectories and metabolic or breathing activity, one can estimate $c_V(\vec{x}_i(t))$ and the exposure dose, d_i, for every individual, and finally, the average probability of infection in the room using Equation (4).

Equation (4) is not in its final form as the virion concentration, $c_V(\vec{\boldsymbol{x}}_i(t))$, is not analytically linked to the virion emission of the infectors or the clean air flow rate. The governing equations for airflow are the Navier–Stokes equations, and there are no general analytical solutions (Berselli, 2021). It is not yet possible to write an analytical formula for $c_V(\vec{\boldsymbol{x}}_i(t))$ in general settings; however, the underlying physical principles can be determined by examining ideal settings.

In cases where all individuals take fixed positions ($\boldsymbol{x_i}$) in a space, e.g., passengers in a bus, train, or aeroplane cabin; students in a classroom; or patrons in a restaurant, and the inhalation exposure during movement from the doorway to position $\boldsymbol{x_i}$ can be ignored, Equation (4) becomes

$$\bar{p}_i = \frac{N_\iota}{N_\sigma} = \frac{1}{N_\sigma}\sum_{i=1}^{N_\sigma}\left(1 - e^{-r_i\int_{t_{1,i}}^{t_{2,i}} q_{in,i}(t)c_V(\boldsymbol{x_i},t)dt}\right). \quad (5)$$

Under steady-state conditions with a constant inhalation rate, a stable virus concentration, and fixed locations, the average infection probability in the space becomes

$$\bar{p}_i = \frac{1}{N_\sigma}\sum_{i=1}^{N_\sigma}\left(1 - e^{-r_i q_{in,i} c_V(\boldsymbol{x_i})\Delta t_i}\right) . \quad (6)$$

If the spatial distributions of the virus concentrations $c_V(\vec{\boldsymbol{x}}_i(t)), c_V(\boldsymbol{x_i}, t)$, or $c_V(\boldsymbol{x_i})$ are known, Equations (4), (5), or (6) can be used, respectively, to estimate the average infection probability of all susceptible individuals in the space, depending on the situation.

In existing outbreak analyses, although susceptible individuals have different exposure times, investigators generally assume an equal dose by using an average exposure time (Li et al., 2021). Investigators also assume a uniform distribution of the virus concentration in space to estimate the infectious quantum emission rate of the infected person. However, the validity of such assumptions has not been analysed, and thus, the assumptions were investigated here.

2.4 Defining effective dilution air and intake fraction time

Estimating individual risk alone does not reveal the intervention mechanisms. We aimed to develop simple indices to compare exposure efficiency at the individual and population levels.

When the infection risk is low, Equation (5) becomes

$$N_\iota \approx N_\sigma \frac{1}{N_\sigma}\sum_{i=1}^{N_\sigma}\left(1 - e^{-r_i\int_{t_{1,i}}^{t_{2,i}} q_{in,i}(t)c_V(\boldsymbol{x_i},t)dt}\right) \approx \sum_{i=1}^{N_\sigma}\left(r_i\int_{t_{1,i}}^{t_{2,i}} q_{in,i}(t)c_V(\boldsymbol{x_i},t)dt\right). \quad (7)$$

Similarly, using Equation (3), the infection probability of individual i becomes

$$p_i(d_i) = 1 - e^{-r_i d_i} \approx r_i\int_{t_{1,i}}^{t_{2,i}} q_{in,i}(t)c_V(\boldsymbol{x_i},t)dt. \quad (8)$$

The number of secondary infections (population risk, Equation 7) and the individual infection probability (individual risk, Equation 8) are affected by parameters related to the infector(s), environment, and susceptible individuals. It is useful to define simple indices to represent the environmental dilution ability during exposure and the overall exposure efficiency as affected by the environment and susceptible individual parameters. These indices are the effective dilution air, q_e, and intake fraction time, $(\mathrm{iF})_t$. q_e is a virtual effective clean air flow rate under pseudo-steady and pseudo-mixing conditions that combines the effects of air volume, air distribution, clean air rate, air change rate and exposure time variability into one variable. $(\mathrm{iF})_t$ may be understood as the effective exposure 'time' of susceptible individuals due to direct inhalation of the expired infectious aerosols via the mouth/nose to mouth/nose without any dilution in the room environment.

Let the estimated number of secondary infections (Equation 7) directly link to the infectious quanta emission rate; thus, we obtain the effective dilution air and intake fraction time. As previously mentioned, when the infectious quantum is used as the infectious unit, $r_i = 1$. In theory, the infectious quantum emission rate can vary for each susceptible individual if a unity value for the dose-response parameter is enforced. For simplicity, we assumed that the emitted quanta rates were constant.

$$N_\iota = (\mathrm{iF})_t N_I Q = N_I Q \frac{1}{q_e} \bar{q}_{in} \overline{\Delta t}, \qquad (9)$$

where intake fraction time $(\mathrm{iF})_t = (\mathrm{iF})\overline{\Delta t}$, $\bar{q}_{in} = \frac{1}{N_\sigma}\sum_{i=1}^{N_\sigma} q_{in,i}$, $\overline{\Delta t} = \frac{1}{N_\sigma}\sum_{i=1}^{N_\sigma} \Delta t_i$, and the intake fraction $(\mathrm{iF}) = \frac{\bar{q}_{in}}{q_e}$. Q is the average infectious quantum emission rate of N_I infectors for all susceptible individuals. In the following text, we also considered a constant inhalation flow rate for all as q_{in}. The effective dilution air q_e is not a physical dilution air flow rate but should be equal to the physical dilution air flow rate at steady-state and uniform conditions. q_e is virtually equivalent to the dilution air (due to indoor ventilation, virus deactivation, particle deposition and filtration) in terms of the dilution effect. Effective dilution air is an inverse linear variable used to determine the number of secondary infections, N_ι, in the same manner as the clean air flow rate, q_p, at steady state and uniform conditions. The concept of effective dilution air allows a direct comparison of *dilution ability* between settings as affected by both the environmental conditions and susceptible individuals.

Our definition of intake fraction time $(\mathrm{iF})_t$ follows an existing concept of intake fraction in exposure science (Bennett et al., 2002). The number of secondary infections, N_ι, is a simple linear function of intake fraction time. The intake fraction time is likely the *simplest* and most *straightforward* parameter linking exposure and source (Equation 9). A lower $(\mathrm{iF})_t$ value leads to a lower level of exposure. One should aim to reduce intake fraction time. The intake fraction (iF) is the *average* ratio of the infectious quantum eventually inhaled by N_σ susceptible individuals to the infectious quantum ($N_I Q \Delta t$) released from N_I infectors. $\frac{q_{in}}{q_e}$ is also known as the rebreathed fraction (Rudnick and Milton, 2003).

We replaced the virion concentration, c_V, with the infectious quantum concentration, c_Q. Combining equations (9) and (7), we obtain

$$(\mathrm{iF})_t N_I Q \approx q_{in} \sum_{i=1}^{N_\sigma} \left(\int_{t_{1,i}}^{t_{2,i}} c_Q(\boldsymbol{x_i}, t) dt \right) \quad \text{and} \quad (10)$$

$$N_I Q \frac{1}{q_e} q_{in} \overline{\Delta t} \approx q_{in} \sum_{i=1}^{N_\sigma} \left(\int_{t_{1,i}}^{t_{2,i}} c_Q(\boldsymbol{x_i}, t) dt \right) . \quad (11)$$

We thus obtain formulas for the effective dilution air, q_e, and the intake fraction time, $(\mathrm{iF})_t$.

$$(\mathrm{iF})_t = \frac{q_{in} \sum_{i=1}^{N_\sigma} \left(\int_{t_{1,i}}^{t_{2,i}} c_Q(\boldsymbol{x_i}, t) dt \right)}{N_I Q} \quad (12)$$

$$q_e = \frac{N_I Q \overline{\Delta t}}{\sum_{i=1}^{N_\sigma} \left(\int_{t_{1,i}}^{t_{2,i}} c_Q(\boldsymbol{x_i}, t) dt \right)} \quad (13)$$

The physics of these two new parameters cannot be obtained directly from Equations (12) and (13). The following ideal setting sheds some light on this problem. If $N_I = 1$ at steady state and with full mixing, $c_Q(\boldsymbol{x_i}) = \frac{Q}{N_\sigma q_p}$, where q_p is the *clean air flow rate* per person, and all susceptible individuals have the same exposure time, Δt ($\overline{\Delta t} = \Delta t$), Equations (12) and (13) can be simplified to Equations (14) and (15).

$$(\mathrm{iF})_t = \frac{q_{in} \sum_{i=1}^{N_\sigma} \left(\int_{t_{1,i}}^{t_{2,i}} c_Q(\boldsymbol{x_i}, t) dt \right)}{Q} = \frac{q_{in}}{q_p} \Delta t \quad (14)$$

$$q_e = \frac{Q \Delta t}{\sum_{i=1}^{N_\sigma} \left(\int_{t_{1,i}}^{t_{2,i}} c_Q(\boldsymbol{x_i}, t) dt \right)} = q_p \quad (15)$$

In such a setting, effective dilution air rate per person, q_e, is simply the clean air flow rate per person, q_p, due to ventilation, virus deactivation, particle deposition and/or filtration. There is a corresponding individual effective dilution air value, $q_{e,i}$, and an individual intake fraction time, $(\mathrm{iF})_{t,i}$, for each susceptible individual i. We then write equation (8) as

$$p_i(d_i) \approx (\mathrm{iF})_{t,i} \frac{1}{N_\sigma} N_I Q \quad \text{and} \quad (16)$$

$$p_i(d_i) \approx N_I Q \frac{1}{N_\sigma q_{e,i}} q_{in,i} \Delta t_i, \quad (17)$$

where $(\mathrm{iF})_{t,i} = (\mathrm{iF}_i) \Delta t_i$, and $(\mathrm{iF}_i) = \frac{q_{in,i}}{q_{e,i}}$. We let

$$p_i(d_i) \approx (\mathrm{iF})_{t,i} \frac{1}{N_\sigma} N_I Q = q_{in,i} \int_{t_{1,i}}^{t_{2,i}} c_Q(\boldsymbol{x_i}, t) dt \quad \text{and} \quad (18)$$

$$p_i(d_i) \approx N_I Q \frac{1}{N_\sigma q_{e,i}} q_{in,i} \Delta t_i = q_{in,i} \int_{t_{1,i}}^{t_{2,i}} c_Q(\boldsymbol{x_i}, t) dt, \quad (19)$$

so that

$$(\mathrm{iF})_{t,i} = \frac{N_\sigma q_{in,i} \int_{t_{1,i}}^{t_{2,i}} c_Q(\boldsymbol{x_i}, t) dt}{N_I Q} \quad \text{and} \quad (20)$$

$$q_{e,i} = \frac{N_I Q \Delta t_i}{N_\sigma \int_{t_{1,i}}^{t_{2,i}} c_Q(\boldsymbol{x_i},t)dt}. \quad (21)$$

Thus, our derivation of individual infection probability (Equation 3) eventually led to the possibility of evaluating 'local' or individual infection risk under different settings and exposure conditions.

2.5 A two-zone setting

To demonstrate the applicability of individual infection probability for understanding non-uniformity, we first estimated infection risk in a reported restaurant outbreak (Li et al., 2021) using a two-zone model. A two-zone model provides analytical solutions under constant-flow conditions (Sinden, 1978, Supplementary Information S5), which enables a detailed investigation of mixing or non-uniformity effects. At least two factors quantitatively contributed to the individual variability in infection in this outbreak, i.e., the arrival and departure time of patrons at each table differed (Table 1) and the local infectious quantum concentration differed by table and individual, although the locations of the patrons were nearly fixed. The effect of individual factors on infection can be considered by the new model. Some patrons may occasionally have stood up, e.g., to pick up food, and their bodies and heads may also have moved during conversation, which would affect both expiration (index case) and inhalation (susceptible individuals). Such minor effects were ignored here, but warrant investigation in future studies.

<**Table 1**>The arrival time, $t_{1,i}$, and departure time, $t_{2,i}$, of patrons at each table

Estimations of the population effective dilution air and intake fraction time need to be specific to the population level being analysed, i.e., the room or a specific zone within the room. One also needs to be mindful that there is a major difference between effective dilution air and intake fraction time, i.e., the effective dilution air is in the denominator (Equation 9; see Supplementary Information S6). Our derivation of individual infection probability (Equation 3) led to the possibility of evaluating the 'local' or individual infection risk under different settings and exposure conditions.\

Based on the restaurant data in Guangzhou, but allowing a larger number of individuals, we set up a hypothetical large but poorly ventilated restaurant divided into two zones (Figure 2B). We do not intend to endorse such a two-zone approach for infection analysis, as in practice, zone division is difficult without detailed CFD or tracer gas measurement data. Our purpose is to use this outbreak to analyse the effect of non-uniformity with analytical solutions. The hypothetical restaurant had an air volume of 1,000 m^3, and 200 people were present (with Zone 1 having 200 m^3 and 40 people and Zone 2 having 800 m^3 and 160 people). The inhalation rate was constant at 0.2 L/s for all patrons. There was only one infector in Zone 1 or 2. The infector emitted a constant quanta generation rate of 150 quanta/h, which was taken from the above-mentioned analysis of the Guangzhou restaurant outbreak. The exposure time of all patrons in each zone satisfied the normal distribution, $N(62, 10.5)$ (units of min). All patrons arrived at the same time as the index case. The index case stayed in the restaurant for 1 h.

<Figure 2>Two-zone division in a restaurant where a COVID-19 outbreak was reported. (A) We divided the restaurant into two sections: Zone 1 or ABC, and Zone 2 or non-ABC. The locations of the tables are only approximate. The seats are shown for Tables A, B, and C, with infected individuals shown in red circles. The numbers in brackets indicate the number of people at each table. The drawing is not to scale. (B) A hypothetical two-zone restaurant with an air volume of 1,000 m^3 and 200 persons present (with 200 m^3 and 40 persons in Zone 1, and 800 m^3 and 160 persons in Zone 2).

The clean air change rate, n_c, included the outdoor air supply, n_0 (ventilation); virus deactivation, n_d; aerosol settling, n_s; and filtration, n_f. The outdoor air supply was 1 L/s per person, so that $n_0 = 0.72$ h^{-1}. $n_c = n_0 + n_d + n_s + n_f = 0.72 + 0.67 + 0.3 + 2 = 3.69$ (h^{-1}). The total clean air flow rates were represented by $q_c = n_c V =$ 1025 L/s and $q_p = 5.125$ L/s per person. The contribution to total clean air by filtration air ($n_f = 2$) is greater than that by ventilation (n_0=0.72). We maintained the mean clean air rate per person, q_p. If all ventilation air, n_0, is in Zone 1, $n_{01} = \frac{1000 \times 0.72}{200} = 3.6$ h^{-1}, whereas if all ventilation air is in Zone 2, $n_{02} = \frac{1000 \times 0.72}{800} = 0.9$ h^{-1}. If all filtration air, n_f, is in Zone 1, $n_{f1} = \frac{1000 \times 2}{200} = 10$ h^{-1}, whereas if all filtration air is in Zone 2, $n_{f2} = \frac{1000 \times 2}{800} = 2.5$ h^{-1}. We used these data to set up scenarios in the hypothetical two-zone restaurant (Table 2).

<**Table 2**>The scenarios in the hypothetical two-zone restaurant

For the fully mixing condition, the number of secondary infections in the hypothetical restaurant was 4.26 (i.e., 4 people). We aimed to analyse the effect of non-uniformity in the two zones on the number of secondary infections under two defined scenarios, i.e., when one zone was better ventilated or filtrated while the other was relatively poorly ventilated or filtrated. The index case was placed in either the poorly diluted or better diluted zone so that the role of exchange flow between the two zones could be studied. We estimated the number of secondary infections in Zones 1 and 2, and the individual and zonal effective dilution air and intake fraction time. For all scenarios, we varied the exchange flow rate between the two zones from 0% to 200% of the total clean air rate of 1025 L/s.

2.6 A simple model of spatial non-uniformity

We further explored the steady-state solution represented in Equation (6) to determine the effect of non-uniform air distribution and to derive an equation to estimate the quanta generation rate, allowing the derivation of a heterogeneous Wells–Riley equation for non-uniform settings.

Under steady-state conditions, all newly released viral particles are removed by ventilation, deposition, filtration, and virus deactivation. The total number of virus particles released by N_I infectors (expiration flow rate $q_{ex,i}$ and virus particle concentration $c_{q,i}$ at the mouth and nose for infector i) is balanced by their removal:

$$\sum_{i=1}^{N_I} q_{ex,i} c_{q,i} = q_c c_e, \qquad (22)$$

where $q_c = q + q_d + q_f + q_s$, and q_c is the combined clean air flow rate due to ventilation, q; virus deactivation, q_d; filtration, q_f; and particle deposition, q_s. c_e is the mean concentration of virus particles at the exhaust(s):

$$c_e = \frac{\sum_{i=1}^{N_I} q_{ex,i} c_{q,i}}{q_c} \tag{23}$$

Note that such an approach is not directly applicable to unsteady-state conditions with non-uniform distribution.

Even under steady-state conditions, with spatial non-uniformity, the concentration, $c_V(\boldsymbol{x_i})$, remains unknown. A local ventilation index, $\varepsilon(\boldsymbol{x_i})$, is defined as the ratio of c_e to the concentration, $c_V(\boldsymbol{x_i})$, at point $\boldsymbol{x_i}$ (Etheridge and Sandberg, 1996, page 268).

$$\varepsilon(\boldsymbol{x_i}) = \frac{c_e}{c_V(\boldsymbol{x_i})} = \frac{\sum_{i=1}^{N_I} q_{ex,i} c_{q,i}}{q_c c_V(\boldsymbol{x_i})} \tag{24}$$

The reciprocal of the local ventilation index is referred to as the susceptible exposure index by Liu et al. (2017). In a fully mixed room, $\varepsilon(\boldsymbol{x_i}) = 1$ in all locations, so that $c_V(\boldsymbol{x_i}) = c_e$. The concentration at any location is the same as the concentration at the exhaust points. The local ventilation index may be greater than one (Liu et al., 2017) and may be a function of the exhalation orientation and the nasal or oral exhalation of the index case (Qian et al., 2008). Air distribution may be designed with a specific local ventilation index distribution, e.g., inverse design methods may be used to design air distribution (Zhai et al., 2014).

Following equations (23-24), we write $c_V(\boldsymbol{x_i}) = \frac{1}{\varepsilon(\boldsymbol{x_i}) q_c} \sum_{i=1}^{N_I} q_{ex,i} c_{q,i}$. If all infectors are equal, $\sum_{i=1}^{N_I} q_{ex,i} c_{q,i} = N_I q_{ex} c_q$. Equation (6) then becomes

$$\bar{p}_i = \frac{N_\iota}{N_\sigma} = 1 - \frac{1}{N_\sigma} \sum_{i=1}^{N_\sigma} \left(e^{-\frac{1}{\varepsilon(\boldsymbol{x_i})} \frac{q_{in,i}}{q_c} (N_I q_{ex} c_q r_i) \Delta t_i} \right). \tag{25}$$

Recognising $Q_i = r_i q_{ex} c_q$, i.e., the total quanta generation rate by an infector for susceptible individual, i,

$$\bar{p}_i = \frac{N_\iota}{N_\sigma} = 1 - \frac{1}{N_\sigma} \sum_{i=1}^{N_\sigma} \left(e^{-\frac{1}{\varepsilon(\boldsymbol{x_i})} \Delta t_i \frac{q_{in,i}}{q_c} N_I Q_i} \right). \tag{26}$$

Note that our derived expired quanta generation rate $Q_i = r_i q_{ex} c_q$ is specific for each susceptible individual. An almost identical equation was used by Buonanno et al. (2020) to estimate quanta from viral load (c_q) data. Our derivation provides the theoretical justification and support for the model described by Buonanno et al. (2020).

In this relatively heterogeneous Wells–Riley model for steady-state conditions, the infectious quanta released by the same infector differ for each susceptible person who is exposed to the infectious viral particles. This difference arises from inter-individual

variability in susceptibility to infection. Most studies of heterogeneity in the infection probability of susceptible individuals have attributed the causes to differences in viral load and contact patterns (Chen et al., 2021). Equation (26) shows that this difference may also be due to variation in the local ventilation index, $\varepsilon(\boldsymbol{x_i})$. The infection probability may be high for someone who stays at a location with an $\varepsilon(\boldsymbol{x_i})$ value much less than 1.

The removal effectiveness of a room contaminant, $\langle\varepsilon\rangle$, was defined based on the average contaminant concentration in the room, $\langle c\rangle$ (Etheridge and Sandberg, 1996, page 267), as follows: $\langle\varepsilon\rangle = \frac{c_e}{\langle c_V(\boldsymbol{x_i})\rangle}$. One may also define the average contaminant removal effectiveness in the breathing zone as $\langle\varepsilon\rangle_{\text{breathing zone}} = \frac{c_e}{\langle c_V(\boldsymbol{x_{i,\text{breathing zone}}})\rangle}$. Here, $\langle\varepsilon\rangle_{\text{breathing zone}}$ is the same zone air distribution effectiveness variable, E_z, as specified in ASHRAE 62.1 (2019). $E_z = 1$ in a room with complete mixing, but can be > 1 in a room ventilated by displacement and < 1 in a room with stagnation, in which the contaminant is 'locked in'. When a stratified air distribution system is used, summer cooling may result in $E_z > 1$, and an E_z value as high as 2 in an auditorium. However, $E_z < 1$ with winter heating (Lee et al., 2009a).

We approximated Equation (26) using the zone air distribution effectiveness variable, E_z, as follows:

$$\bar{p_i} = \frac{N_\iota}{N_\sigma} = 1 - \frac{1}{N_\sigma}\sum_{i=1}^{N_\sigma}\left(e^{-\frac{1}{E_z}\Delta t_i \frac{q_{in,i}}{q_c} N_I Q_i}\right). \qquad (27)$$

Equation (27) is a useful model that uses the zone air distribution effectiveness of ASHRAE 62.1 (2019) directly, while considering the individual probability of infection. The model represented in Equation (27) may be further simplified into the standard Wells–Riley equation (Riley et al., 1978) by considering the situation when $E_z = 1$, and all susceptible individuals are equal.

$$\bar{p_i} = \frac{N_\iota}{N_\sigma} = 1 - e^{-N_I Q \frac{q_{in}}{q_c}\Delta t} \qquad (28)$$

3.Rsults

3.1 *Two-zone analysis of a restaurant outbreak*

We demonstrated our theory in a restaurant outbreak of COVID-19 (Li et al., 2021). If the whole restaurant was considered as a single space studied (Method 1 in Table 3), a steady-state estimation resulted in a quanta generation rate of 132.2 h^{-1}. However, considering the transient effect, the quanta generation rate is 154.9 h^{-1}. Considering the ABC zone as an 'isolated' space (Method 2 in Table 3, Parhizkar et al., 2021), we obtained estimated quanta emission rates of 136.7 h^{-1} and 164.3 h^{-1} for the steady-state and transient settings, respectively. The ABC zone estimates were reasonably close to the whole restaurant estimates. Why does the ABC zone approach work in this setting? To answer this question, we further considered a two-zone approach, i.e., the ABC and non-ABC zones, with an estimated exchange airflow rate

between the two zones of 280 L/s (Table S1) based on tracer gas monitoring data reported by Li et al. (2021).

<**Table 3**>Estimation of the infectious quantum emission rate when the zonal or total space is assumed to be fully mixed

We used the analytical solutions of the two-zone model (Supplementary Information S5) to estimate the spatiotemporal distribution of virus concentrations in the two zones. Exposure level of each susceptible individual was estimated based on their location (the ABC or non-ABC zone) and their arrival and departure times. Hence, individual infection probability was considered. The exact arrival and departure times of patrons at different tables were determined from closed-circuit television video footage (Li et al., 2021). By the time the patrons at Table A arrived, most patrons had already arrived, except those at Table C (2 min later), Table 08 (27 min), Table 12 (12 min), and Table 17 (59 min). By the time the patrons at Table A departed, those at some other tables remained, including those at Table 08 (14 min more), Table 10 (5 min), Table 15 (7 min), and Table 17 (56 min, the last to leave). There were significant variations in exposure time and timing (starting and ending time). As those at Table A stayed for 82 min, the concentration did not reach full steady-state conditions by the time they left. There was a decay period in virus concentration when the remaining tables continued to be exposed.

To distinguish the contributions of spatial non-uniformity and exposure variability, we first used the average exposure time in Methods 3 and 4 (Table 3), which assumed that secondary infections may occur in the whole restaurant or only in the ABC zone, respectively. The predicted quanta generation rate was 369.0 h^{-1} when considering the temporal variation in virus concentration using Method 4. A significant error occurred, as secondary infections were also likely to occur in the non-ABC zone. We further used the individual exposure time (with the detailed arrival and departure times listed in Table 1). The two-zone model using the individual exposure time and focusing on the whole restaurant (Method 5) predicted a quanta generation rate of 152.1 h^{-1}. However, when focusing on the ABC zone (Method 6), the predicted quanta generation rate of 368.8 h^{-1} appeared to be over-estimated.

A comparison of the predicted quanta generation rates using Methods 3 and 5 suggested that the effect of using the arithmetic average of the exposure time was a reasonable approach. However, this conclusion is only valid when there is no variation in the inhalation rate. When variations exist in both the inhalation rate and exposure time, errors may be expected. However, this requires further investigation.

To further examine the observed differences in predicted quanta generation rates using the six different methods listed in Table 3, we predicted the number of secondary infections in the ABC zone, the non-ABC zone, and the whole restaurant, as the exchange air flow between two zones varied (Figure 3).

<**Figure 3**> **Infection outbreak in the restaurant in Guangzhou analysed using a two-zone model.**

The mixing between ABC and non-ABC zones was reasonably significant at the time of exposure when the outbreak occurred (shown by the vertical green line in Figure

3A). This explains why both the whole-zone and the single-ABC approaches (Methods 1 and 2) produced similar infectious quantum emission rates. However, when the ABC zone was assumed to produce the nine secondary infections, and both zones were included in the analysis, a quanta generation rate greater than 330 quanta/h was predicted (Methods 4 and 6). The exchange airflow from the relatively clean non-ABC zone to the ABC zone helps dilute the virus-containing aerosols in the ABC zone (Figure 3C). To achieve the same number of secondary infections, a higher quanta generation rate is needed. Note that a similar number of secondary infections occurred in the ABC and non-ABC zones if based on an estimated exchange airflow rate of 280 L/s.

The restaurant at which the outbreak occurred had two relatively 'balanced' ABC and non-ABC zones, i.e., the population risks in the two zones were approximately equal (Figure 3A or 3B), although the dilution capability was greater in the non-ABC zone than the ABC zone (Figure 3C). There was relatively good mixing between the two zones at the time of the COVID-19 outbreak. However, the situation differs when the inter-zonal exchange flow is low. All secondary infections would occur in the ABC zone when the exchange airflow was less than 20 L/s. At a possible exchange air flow rate of 280 L/s, half of the secondary infections would occur in the ABC zone and half would occur in the non-ABC zone, although the total number of secondary infections would remain the same. Movement of the index case between the ABC zone and the non-ABC zone would not lead to an increase in the total number of secondary infections with a quanta generation rate of 152.1 h^{-1}. This also explains why Method 2 accurately described the outbreak. The analogue method, Method 6, produced almost double the number of secondary infections in the entire restaurant.

The predicted effective dilution air of the total restaurant was approximately 10 L/s per person, which was slightly higher than the combined clean air flow rate of 7.6 L/s per person. The overall effective dilution air and overall intake fraction time varied little when the exchange flow varied. Note that the effect of the inter-zonal exchange flow on the overall intake fraction time did not fully follow its effect on the number of secondary infections due to the linear approximation used in Equation 7 when the infection risk was relatively large. If the intake fraction time is defined without a linear approximation, the disagreement disappears (not shown here). The number of secondary infections in the total restaurant remained relatively constant at nine cases when the quanta generation rate was 152.1 h^{-1}, as the exchange flow changed from 20 L/s to 6,000 L/s.

There was a significant decrease in the total number of secondary infections in the restaurant at a quanta generation rate of 368.8 h^{-1} when the exchange flow was low. With this quanta generation rate, the expected total number of secondary infections in the restaurant increased from 16 to 19 as the exchange flow increased from 20 L/s to 280 L/s (red line in Figure 3A). Such an effect was further analysed using a hypothetical two-zone restaurant, in which the clean air rates per person due to outdoor airflow and filtration differed in the two zones.

3.2 *Non-uniformity*

The values of E_z are given in ASHRAE 62.1 (2019, Table 6-2) for typical air distribution systems, with a large range of 0.7–1.5 (Figure 4). In the worst-case

scenario considered in ASHRAE 62.1 (2019), in which warm air is supplied into a room with ceiling exhaust, $E_z = 0.7$. In a displacement ventilated room, the application of personalised ventilation would lead to $E_z = 1.5$. Other air distribution systems have E_z values between those of these two systems.

<Figure 4>Air distribution effectiveness in the breathing zone for typical air distribution systems.

Equation (27) may be simplified at a low infection probability and constant inhalation rate, exposure time, and quanta emission rate to $\bar{p}_i = \frac{N_\iota}{N_\sigma} \approx \frac{N_I Q}{E_z} \Delta t \frac{q_{in}}{q_c}$. The number of secondary infections then becomes $N_\iota \approx \frac{N_I Q}{E_z} \Delta t \frac{q_{in}}{q_p}$. Assuming that all other parameters are identical, a difference of 0.7–1.5 in the E_z value results in more than a 100% difference in the number of secondary infectionsv.

The contaminant removal effectiveness, $\varepsilon(\boldsymbol{x_i})$, depends on the spatial location $\boldsymbol{x_i}$. The use of the E_z values reported in ASHRAE 62.1 (2019) may be problematic in some situations. For example, in a displacement ventilated room, $\varepsilon(\boldsymbol{x_i})$ = 1 in the upper mixing zone but may be much greater than 1 if the susceptible individual inhales from the lower clean zone. As an example, consider 50% of N_σ (even number) individuals in a room with $\varepsilon(\boldsymbol{x_L}) = 1.30$ and their heads below the clean zone height, and 50% of N_σ individuals in the same room with $\varepsilon(\boldsymbol{x_U}) = 0.96$ and their heads above the clean zone height (Lee et al., 2009a).

$$N_\iota = \sum_{i=1}^{0.5N_\sigma} \left(1 - e^{-\frac{1}{\varepsilon(\boldsymbol{x_L})} \Delta t_i \frac{q_{in,i}}{q_c} N_I Q_i}\right) + \sum_{i=0.5N_\sigma+1}^{N_\sigma} \left(1 - e^{-\frac{1}{\varepsilon(\boldsymbol{x_U})} \Delta t_i \frac{q_{in,i}}{q_c} N_I Q_i}\right) \quad (29)$$

When the infection probability is low and each susceptible individual is identical for exposure parameters (i.e., $q_{in,i} = q_{in}$, $\Delta t_i = \Delta t$ and $Q_i = Q$), the average number of secondary infections becomes

$$N_\iota \approx \frac{1}{2} N_\sigma \frac{1}{\varepsilon(\boldsymbol{x_L})} \Delta t \frac{q_{in}}{q_c} N_I Q + \frac{1}{2} N_\sigma \frac{1}{\varepsilon(\boldsymbol{x_U})} \Delta t \frac{q_{in}}{q_c} N_I Q. \quad (30)$$

Substituting two-contaminant removal effectiveness into Equation (30), we obtain $N_\iota \approx 0.91 N_I Q \frac{q_{in}}{q_p} \Delta t$. Thus, the number of secondary infections, N_ι, becomes 9% fewer in such a room ventilated by displacement rather than by mixing ventilation. Without using CFD, it is not possible to determine the effect of the location of the breathing zone of infectors (below or above the clean zone height). Note that displacement ventilation may enhance short-range airborne transmission (Liu et al., 2019). The result of Equation (30) only applies to long-range airborne exposure.

The E_z approach may be easily applied to airborne infection risk assessment following our derivation. This is done by assuming a uniform level of 'non-uniformity' (i.e., uniform contaminant removal effectiveness $\varepsilon(\boldsymbol{x_i})$ in the breathing zone). However, in practice, a room may have multiple zones with different concentration distributions. A simple model is depicted in Figure 5, in which a long room may be divided into two zones – one with good dilution and another with poor dilution. Such a model is similar to the scenario in the restaurant and cannot be analysed using the

E_z approach. Thus, a two-zone (or multi-zone) approach may be a good model to handle this issue.

<Figure 5>A long room with a two-zone air distribution mode.

3.3 *Infection spread between two non-uniform zones*

The non-uniformity of clean air distribution between two zones in a room and the exchange airflow between the two zones are also important for airborne infections. For the two basic scenarios in Table 2, we imposed uniformity in the dilution ratio per person in and between the two zones. The exchange airflow between the two zones did not significantly change the overall number of secondary infections in the hypothetical restaurant (basic scenarios 01 and 02 in Figure 6A and 6B), i.e., with approximately four individuals infected. This confirmed the findings in the restaurant model described in Section 3.1. Of note, when Zone 1 is poorly ventilated (Figure 6A, case 14) or poorly filtrated (Figure 6B, case 34), an index case in the better-ventilated or better-filtrated Zone 2 would lead to the same number of secondary infections as the two basic scenarios.

<Figure 6>Infection risk assessment in a hypothetical two-zone restaurant considering the effects of clean air distribution and inter-zonal air mixing.

However, when the index case is in poorly ventilated Zone 2 (Figure 6A, case 13) or poorly filtrated Zone 2 (Figure 6B, case 33), in which there are three times more susceptible individuals than in Zone 1, the total number of secondary infections increases to a maximum of five and seven individuals, respectively. These were the greatest numbers of secondary infections of all tested cases listed in Table 2. The corresponding intake fraction time was also the greatest for cases 13 and 33, whereas the effective dilution air for these two cases was the least among all tested cases.

The least number of secondary infections occurred when the index case was in the better-ventilated or better-filtrated Zone 1, in which there was a small number of susceptible individuals (Figure 6A1, case 11 and Figure 6B1, case 31). The smallest number of secondary infections occurred when there was a minimum exchange flow between the two zones, i.e., three secondary infections in case 11 and only two secondary infections in case 31. These cases represent a 25% and 50% reduction, respectively, from four secondary infections in the fully mixing condition. The corresponding intake fraction time was the least and the effective dilution air was the greatest for cases 11 and 31 amongst all the test cases presented in Figure 6A and 6B.

For a fully mixing condition with four secondary infections, non-uniformity led to a change in the number of secondary infections to 3–5 when ventilation was not uniformly distributed (Figure 6A1), and to a wider range of 2–7 when filtration was not uniformly distributed (Figure 6B1). The difference between the two ranges was caused by the difference in the clean air flow rate due to ventilation and filtration. The widest range occurred when the exchange flow rate between the two zones was the lowest. As the exchange flow rate increased, the difference in the number of secondary infections contributed by non-uniform ventilation or filtration became smaller. Thus, enhanced inter-zonal mixing led to better uniformity in both virus

concentration (Figure 7A1, 7B1) and the number of secondary infections (Figure 6A1, 6B1).

<Figure 7>Infection risk assessment in a hypothetical two-zone restaurant with the index case in Zone 1 for scenarios 01 and 31.

In summary, when all other parameters were identical, an index case in a less-populated zone led to fewer secondary infections, and better dilution in the zone where the index case was located minimised the total number of secondary infections. When crowding and dilution were uniform between zones, inter-zonal mixing did not significantly affect the total number of secondary infections. However, when the index case was in a poorly diluted zone, greater inter-zonal mixing significantly decreased the total number of infections. In contrast, when the index case was in a well-diluted zone with a smaller population, greater inter-zonal mixing increased the total number of infections.

We further compared the detailed zonal parameters between basic scenario 01 and scenario 31 in Figure 7A and Figure 7B. The zonal parameters in both scenarios and the overall parameters (room scale) in case 31 changed significantly with the increasing exchange flow rate between the two zones. The overall parameters (room scale) in basic scenario 01 remained unchanged basically with the increasing exchange flow rate between the two zones, due to two equally diluted zones in case 01. In both scenarios, the overall parameters showed a similar trend to the parameters of Zone 2 and the opposite trend to the parameters of Zone 1, as the index case stayed in Zone 1. Both the number of secondary infections and the intake fraction time satisfied the arithmetic sum rule (Zone 1 + Zone 2 = overall room, Equation S49), but effective dilution air satisfied the harmonic mean (Equation S50). Despite the greatest overall effective dilution air (Figure 7B4) and the shortest overall intake fraction time (Figure 7B3), case 31 presents the lowest concentration of infectious quanta in both zones (Figure 7B1). This resulted in the least number of secondary infections when the exchange flow rate was lowest or zero. Our model also allowed the examination of individual infection probability (Figure S1).

4.Discussion

The most significant effect of non-uniformity is the resulting inter-individual variability in airborne exposure. Such heterogeneity affects both the individual infection risk and population infection risk in the space (indicated by the number of newly infected individuals). Our derived heterogeneous Wells–Riley equation, $\bar{p}_i = \frac{N_\iota}{N_\sigma} = 1 - \frac{1}{N_\sigma}\sum_{i=1}^{N_\sigma}\left(e^{-\frac{1}{\varepsilon(x_i)}\Delta t_i \frac{q_{in,i}}{q_c} N_I Q_i}\right)$, enabled us to understand the effect of spatial non-uniformity and the combined effects of spatial non-uniformity and temporal and exposure time variability on infection risk. This new Wells–Riley equation was derived using the Poisson-binomial distribution (Bogen and Spear, 1987; Nicas, 1996).

Heterogeneity also exists in the viral load released, number of contacts (e.g., the number of people in a room), contact effectiveness (e.g., frequency of close contact or dilution ability), and susceptibility level of susceptible individuals. All of these factors lead to over-dispersion in the transmissibility of emerging respiratory viruses

(Lloyd-Smith et al., 2005; Chen et al., 2021). Our derived general dose-response model, $\frac{N_\iota}{N_\sigma} = \bar{p}_i = 1 - \frac{1}{N_\sigma}\sum_{i=1}^{N_\sigma}(e^{-r_i d_i})$, offers an approach for further investigations of over-dispersion. This was not investigated in the current study, as we focused on the non-uniformity effect. Our idea of following the trajectory of a susceptible individual allowed us to estimate the *individual* inhalation probability of a virus particle (virion) in space, which provided a direct link between the traditional Wells–Riley equation and the dose-response model(s). Our derived formula for infectious quantum emission is suitable for susceptible individual-based analyses and provides theoretical support for the formula first proposed by Buonanno et al. (2020).

We demonstrated that the new model offers the possibility to consider spatial non-uniformity when studying heterogeneity and paves the way to explore which factor(s) play the most important role. This understanding is essential for designing interventions, particularly for ventilation and air distribution. The question remains: is infection heterogeneity virological, behavioural, or environmental? That is, is infection heterogeneity mainly due to heterogeneity in the virus, the susceptible individuals, or the environment? Heterogeneity is possible in both the dose-response parameter, r_i, and the exposure dose, d_i. r_i relates to the heterogeneity in susceptibility, but d_i relates to the heterogeneity in the viral load released, inhalation rate (less variation), exposure time, spatiotemporal non-uniformity, and viral aerosol dilution (e.g., heterogeneity in the ventilation rates). Our study shows that one cannot ignore the effect of spatial non-uniformity. It also indicates that non-uniformity is an important parameter in airborne outbreak investigations. There have been many engineering studies of the air distribution effect on inhalation exposure (e.g., Sze To et al., 2008). However, data from these studies cannot be used directly to estimate the average number of secondary infections when there is non-uniformity. Our derived heterogeneous Wells–Riley equation offers a framework for systematic studies of airborne infection risk with individual variability, while accounting for the non-uniformity effect.

Our data show that dead or less-diluted zones in a space may be risky when an index case is present in these zones. In our modelling study, an index case in a relatively isolated and well-diluted zone causes fewer secondary infections when there is minimum mixing between the two zones than when there is sufficient inter-zonal mixing. However, mixing or exchange airflow between two zones may have dual effects. It may have a diluting effect if the source air is relatively clean, thus decreasing the number of secondary infections, or it may have a contaminating effect if the source air is relatively contaminated, thus increasing the number of secondary infections.

An infector in a poorly diluted zone with many susceptible individuals increases the risk of infection relative to the risk of infection when an infector is in a well-diluted zone with few susceptible individuals (Figure 8). In the former setting, inter-zonal mixing leads to a decrease in the total number of infections, whereas in the latter setting, inter-zonal mixing leads to an increase in the total number of infections. In general, the non-uniformity effect is complicated by variations in crowding, dilution capacity, the location of the index case, and exchange airflow. The two-zone non-mixing data presented in Figure 6 and Figure 7 offer important insights into infection control. For example, a designated ‘fever area’ may be created in an

emergency department during a pandemic period (Wee et al., 2020). The observed fewer overall secondary infections in a hypothetical two-zone restaurant with the infector in a well-diluted zone (Figure 6) suggests the usefulness of keeping a 'fever area' well diluted and isolated.

<**Figure 8**>

This study on mixing between two zones was supplemented by introducing two relatively new concepts, i.e., the intake fraction time and effective dilution air. These concepts are useful in explaining how the number of secondary infections changes as environmental factors. The population intake fraction time $(\mathrm{iF})_t$ directly measures the effective exposure time of susceptible individuals due to direct inhalation of the expired infectious aerosols via the mouth/nose to mouth/nose without any dilution in the room environment. As $N_t = (\mathrm{iF})_t N_I Q < 1$, then $(\mathrm{iF})_t < \frac{1}{N_I Q}$. The definition of this parameter shows that it may be the simplest single parameter to measure the combined effects of the environment and susceptible individuals on airborne infections. When the emitted infectious quanta rate is known, the allowable maximum intake fraction time to avoid a secondary infection is also known. The intake fraction time is a collective parameter that includes the effects of the environment and susceptible individual parameters on infection risk. We also defined the effective dilution air (q_e) at pseudo-steady and mixing conditions by $(\mathrm{iF})_t = \frac{1}{q_e}\bar{q}_{in}\overline{\Delta t}$, which is a simple parameter that measures the effective dilution ability of the space environment based on the clean air flow rate (including ventilation, virus deactivation, particle deposition, and filtration), air distribution, air volume and transient factors. The effective dilution air parameter, q_e, is a surrogate for the dilution ability of the environment. It is uniquely defined for an individual or population of individuals in a room for a certain period of exposure. Infection control in a space setting must consider everyone in the space, including residents and/or visitors. The individual effective dilution air is a useful concept. It extends from ventilation air to all dilution air and includes the effect of exposure time and timing related to the presence of the index case. Residents and visitors have different exposure times and timing. We expect that these two simple concepts will find more applications in the study of airborne transmission.

For the restaurant outbreak in Guangzhou, our analysis showed that only a 20 L/s inter-zonal exchange flow would have prevented secondary infections in the non-ABC zone (Figure 3A). It is difficult to imagine that the exchange air flow between two zones in such an open space can be as low as 20 L/s (Li et al., 2021). However, it was not possible to reconstruct the airflow conditions at the time of exposure. The number of asymptomatic infections was also unknown at the time of the investigation (as it was very early in the pandemic). However, based on data obtained from the original research team (Li et al., 2021), there appears to have been a reasonable amount of mixing in the restaurant. The fully mixing model (Method 1, Table 3) provided a reasonable estimate of the quanta generation rate, but the locations where half of the secondary infections occurred were incorrect. Based on this result, some people in the non-ABC zone appear to have been infected, however, this was not observed. Our reanalysis of the outbreak revealed the difficulty in reproducing the exposure setting at the time of an airborne outbreak. This restaurant outbreak provided 'a well-documented' COVID-19 outbreak 'with significant

meta-data available for purposes of model application' (Parhizkar et al., 2021), but our analysis shows that the description is incomplete. An airborne outbreak investigation needs to consider non-uniformity. The new individual risk assessment model for airborne infections developed here will provide a practical tool for future outbreak investigations.

Our rigorous derivation shows that the existing zone air distribution effectiveness of ASHRAE 62.1 (2019) may be used to estimate the effect of air distribution on airborne infection risk. We first used the contaminant removal effectiveness parameter, $\varepsilon(\boldsymbol{x_i})$, and obtained an average value in the breathing zone identical to the E_z value (ASHRAE 62.1, 2019; Lee et al., 2009b). Though not as well known, the concept of 'ventilation effectiveness', E_z, was first proposed by Yaglou and Witheridge (1937). The advantage of our derived formula is that it directly links our threshold dilution airflow rate for a respiratory infection to the commonly used ventilation effectiveness in the current minimum ventilation standards for indoor air quality.

Our work has several major limitations. The first and most important limitation is that the non-uniformity effect was studied in isolation, without considering heterogeneity in susceptibility. Heterogeneity in susceptibility has been widely studied in the virology and public health fields, which do not typically include the study of non-uniformity. Our derived general dose-response model offers the possibility of studying the non-uniformity effect and heterogeneity in susceptibility together, and when data become available, such a study will become a reality in outbreak investigations. The second limitation is that only a single virion was considered per aerosol; thus, the probability of inhaling a single virion was estimated. However, one aerosol may contain multiple virions, and inhaling aerosols containing multiple virions differs from inhaling single-virion aerosols. With ten virions, 10 single-virion aerosols may be inhaled by 10 people, while a 10-virion aerosol can only be inhaled by one person. Thus, multi-virion aerosols impact on airborne infection risk. This complex topic will be addressed in a future study.

5.Conclusions

The effect of infectious aerosol concentration non-uniformity on airborne infection risk was studied by considering inter-individual variability in inhalation exposure. By following the trajectory of a susceptible individual in a room, the *individual* inhalation probability of a virus particle (or virion) in space was estimated for the first time. This estimation enabled the derivation of a new general dose-response model and heterogeneous Wells–Riley equation for airborne infections using the single-hit model and Poisson-binomial distribution. The new heterogeneous Wells–Riley model showed that the existing zone air distribution effectiveness of ASHRAE 62.1 (2019) may be linked to spatial non-uniformity for airborne infection risk assessment, and that the modelling of the quanta generation rate by Buonanno et al. (2020) is theoretically justified. When there is uniformity in the zonal clean air rate per person, inter-zonal air mixing does not change the number of secondary infections in the space. However, when there is significant difference in clean air rate per person between the two zones, inter-zonal air mixing may either increase or decrease the number of secondary infections in the space, depending on the setting. Our data

suggest that future airborne outbreak investigations should consider airflow non-uniformity.

Funding

This work was supported by a Collaborative Research Fund provided by the Research Grants Council of Hong Kong (grant number C7124-21E).

Data availability

No data was used for the research described in the article.

Acknowledgements

The authors appreciate the insightful and stimulating comments on the inter-zonal mixing effect, as described in the Introduction, from Professor Pawel Wargocki of the Technical University of Denmark, Professor Julian Tang of the University of Leicester, and other colleagues when the work by Li et al. (2021) was first presented in mid-2020.

References

J.W. Tang, R. Tellier, Y. L(2022). Hypothesis: all respiratory viruses (including SARS.CoV-2) are aerosol-transmitted.*Indoor Air,*32(1),e12937.

World Health Organization (WHO), Hazard characterization for pathogens in food and water: guidelines (No. 3), Food Agric. Organ. (2003) 27–39.

C.N. Haas, Action levels for SARS-CoV-2 in air: preliminary approach, Risk Anal. 41 (5) (2021) 705–709.

E.C. Riley, G. Murphy, R.L. Riley, Airborne spread of measles in a suburban elementary school, Am. J. Epidemiol. 107 (5) (1978) 421–432.

L. Gammaitoni, M.C. Nucci, Using a mathematical model to evaluate the efficacy of TB control measures, Emerg. Infect. Dis. 3 (3) (1997) 335–342.

S.N. Rudnick, D.K. Milton, Risk of indoor airborne infection transmission estimated from carbon dioxide concentration, Indoor Air 13 (3) (2003) 237–245.

H. Parhizkar, K.G. Van Den Wymelenberg, C.N. Haas, R.L. Corsi, A Quantitative Risk Estimation Platform for Indoor Aerosol Transmission of COVID-19. Risk Analysis, 2021, https://doi.org/10.1111/risa.13844, issue not assigned.

S.M. Moghadas, T.N. Vilches, K. Zhang, C.R. Wells, A. Shoukat, B.H. Singer, L.A. Meyers, K.M. Neuzil, J.M. Langley, M.C. Fitzpatrick, A.P. Galvani, The impact of vaccination on coronavirus disease 2019 (COVID-19) outbreaks in the United States, Clin. Infect. Dis. 73 (12) (2021) 2257–2264.

G.N. Sze To, C.Y.H. Chao, Review and comparison between the Wells-Riley and dose-response approaches to risk assessment of infectious respiratory diseases,Indoor Air 20 (1) (2010) 2–16.

G.N. Sze To, M.P. Wan, C.Y.H. Chao, F. Wei, S.C.T. Yu, J.K.C. Kwan,A methodology for estimating airborne virus exposures in indoor environments using the spatial distribution of expiratory aerosols and virus viability characteristics, Indoor Air 18 (5) (2008) 425–438.

H. Qian, Y.Li, P.V. Nielsen, X. Huang, Spatial distribution of infection risk of SARS transmission in a hospital ward, Build. Environ. 44 (8) (2009) 1651–1658.

Y.Li,H.Qian,J.Hang,X.Chen,P.Cheng,H.Ling,S.Wang,P.Liang,J.Li,S.Xiao,J.Wei, Probable airborne transmission of SARS-CoV-2 in a poorly ventilated restaurant, Build.Environ.196 (2021),107788.

P.V. Nielsen, A. Restivo, J.H. Whitelaw, The velocity characteristics of ventilated rooms, J. Fluid Eng. 100 (3) (1978) 291–298.

D.W. Etheridge, M. Sandberg, Building Ventilation: Theory and Measurement, vol. 50, John Wiley & Sons, Chichester, UK, 1996.

K.T. Bogen, R.C. Spear, Integrating uncertainty and interindividual variability in environmental risk assessment, Risk Anal. 7 (4) (1987) 427–436.

C.N.Haas,Estimation of risk due to low doses of microorganisms:a comparison of

alternative methodologies, Am. J. Epidemiol. 118 (4) (1983) 573–582.

M. Nicas, An analytical framework for relating dose, risk, and incidence: an application to occupational tuberculosis infection, Risk Anal. 16 (4) (1996) 527–538.

H.J. Miller, Modelling accessibility using space-time prism concepts within geographical information systems, Int. J. Geogr. Inf. Syst. 5 (3) (1991) 287–301.

L.C. Berselli, Three-Dimensional Navier-Stokes Equations for Turbulence, Academic Press, London, UK, 2021.

D.H. Bennett, M.D. Margni, T.E. McKone, O. Jolliet, Intake fraction for multimedia pollutants: a tool for life cycle analysis and comparative risk assessment, Risk Anal. 22 (5) (2002) 905–918.

F.W. Sinden, Multi-chamber theory of air infiltration, Build. Environ. 13 (1) (1978) 21–28.

L.Liu,Y.Li,P.V.Nielsen,J.Wei,R.L.Jensen,Short-range airborne transmission of expiratory droplets between two people, Indoor Air 27 (2) (2017) 452–462.

H.Qian,Y.Li,P.V.Nielsen,C.E.Hyldgaard,Dispersion of exhalation pollutants in a two-bed hospital ward with a downward ventilation system, Build. Environ. 43 (3) (2008) 344–354.

Z.J.Zhai,Y.Xue,Q.Chen, Inverse design methods for indoor ventilation systems using CFD-based multi-objective genetic algorithm, Build. Simulat. 7 (6) (2014) 661–669.

G.Buonanno, L.Stabile, L.Morawska, Estimation of airborne viral emission: quanta emission rate of SARS-CoV-2 for infection risk assessment, Environ. Int. 141 (2020), 105794.

P.Z.Chen,N.Bobrovitz,Z.Premji,M.Koopmans,D.N.Fisman,F.X.Gu, Heterogeneity in transmissibility and shedding SARS-CoV-2 via droplets and aerosols, Elife 10 (2021), e65774.

ASHRAE 62.1, ANSI/ASHRAE Standard 62.1-2019, Ventilation for Acceptable Indoor Air Quality, American Society of Heating, Refrigerating and AirConditioning Engineers, Inc, Atlanta, GA, 2019.

K.S.Lee,T.Zhang,Z.Jiang,Q.Chen,Comparison of airflow and contaminant distributions in rooms with traditional displacement ventilation and under-floor air distribution systems, ASHRAE Transactions 115 (2) (2009) 306–321.

F.Liu,C.Zhang, H.Qian,X.Zheng,P.V.Nielsen,Direct or indirect exposure of exhaled contaminants in stratified environments using an integral model of an expiratory jet, Indoor Air 29 (4) (2019) 591–603.

J.O.Lloyd-Smith,S.J.Schreiber,P.E. Kopp,W.M.Getz,Superspreading and the effect of individual variation on disease emergence, Nature 438 (7066) (2005) 355–359.

L.E.Wee,T.P.Fua,Y.Y.Chua,A.F.Ho,X.Y.Sim,E.P.Conceicao,I.Venkatachalam, K.B.K. Tan, B.H. Tan, Containing COVID-19 in the emergency department: the role of improved case detection and segregation of suspect cases, Acad. Emerg. Med. 27 (5) (2020) 379–387.

K.S.Lee,Z.Jiang,Q.Chen,Air distribution effectiveness with stratified air distribution systems, ASHRAE Transactions 115 (2009) 322.

C.P. Yaglou,W.N.Witheridge,Ventilation requirements,Part 2,ASHRAE Transactions 42 (1937) 423–436.

P.V.Nielsen,A.Restivo,J.H.Whitelaw, Buoyancy-affected flows in ventilated rooms, Numer. Heat Transf. 2 (1) (1979) 115–127.

J.J.Costa, L.A.Oliveira,D. Blay,Turbulent airflow in a room with a two-jet heating-ventilation system — a numerical parametric study, Energy Build. 32 (3) (2000) 327–343.

C.Topp,P.V.Nielsen,P.Heiselberg, Influence of local airflow on the pollutant emission from indoor building surfaces, Indoor Air 11 (3) (2001) 162–170.

B.Tripathi,S.G.Moulic,Investigation of the buoyancy affected airflow patterns in the enclosure subjected at the different wall temperatures, Energy Build. 39 (8) (2007) 906–912.

Figure 1

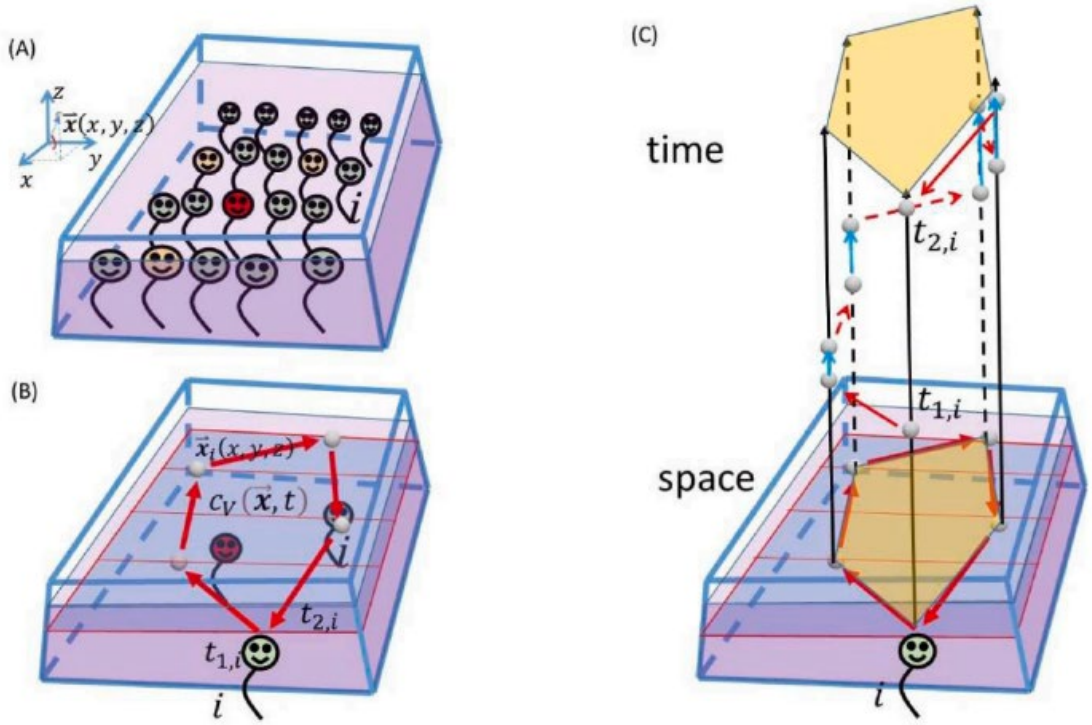

Figure 2

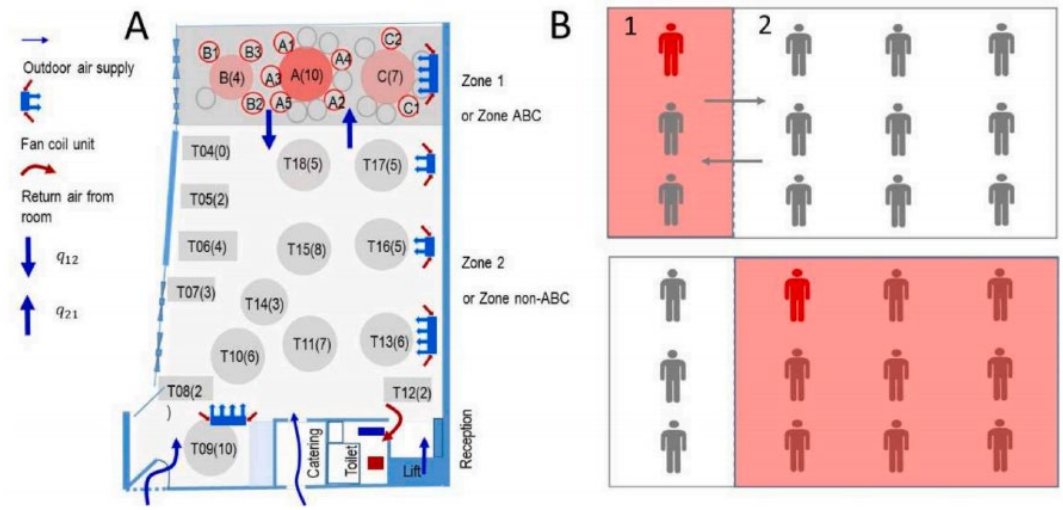
A
Outdoor air supply
Fan coil unit
Return air from room
q_{12}
q_{21}
B1
B3
A1
C2
B(4)
A3
A(10)
A4
C(7)
B2
A5
A2
C1
T04(0)
T18(5)
T17(5)
T05(2)
T06(4)
T15(8)
T16(5)
T07(3)
T14(3)
T10(6)
T11(7)
T13(6)
T08(2)
T12(2)
T09(10)
Catering
Toilet
Lift
Reception
Zone 1
or Zone ABC
Zone 2
or Zone non-ABC
B
1
2

Figure 3

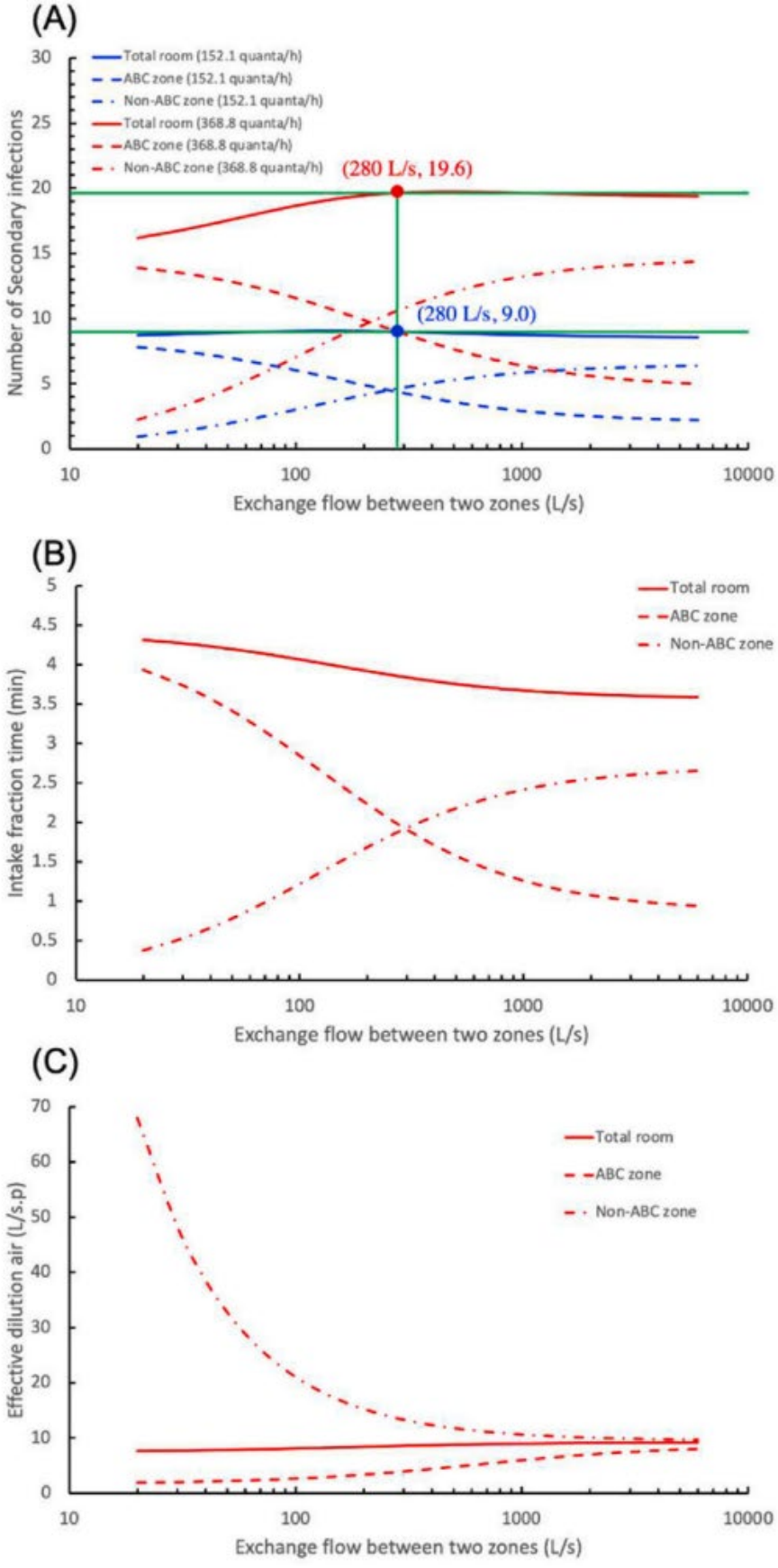
(A)
Total room (152.1 quanta/h)
ABC zone (152.1 quanta/h)
Non-ABC zone (152.1 quanta/h)
Total room (368.8 quanta/h)
ABC zone (368.8 quanta/h)
Non-ABC zone (368.8 quanta/h)
(280 L/s, 19.6)
(280 L/s, 9.0)
Number of Secondary infections
Exchange flow between two zones (L/s)
(B)
Total room
ABC zone
Non-ABC zone
Intake fraction time (min)
Exchange flow between two zones (L/s)
(C)
Total room
ABC zone
Non-ABC zone
Effective dilution air (L/s.p)
Exchange flow between two zones (L/s)

Figure 4

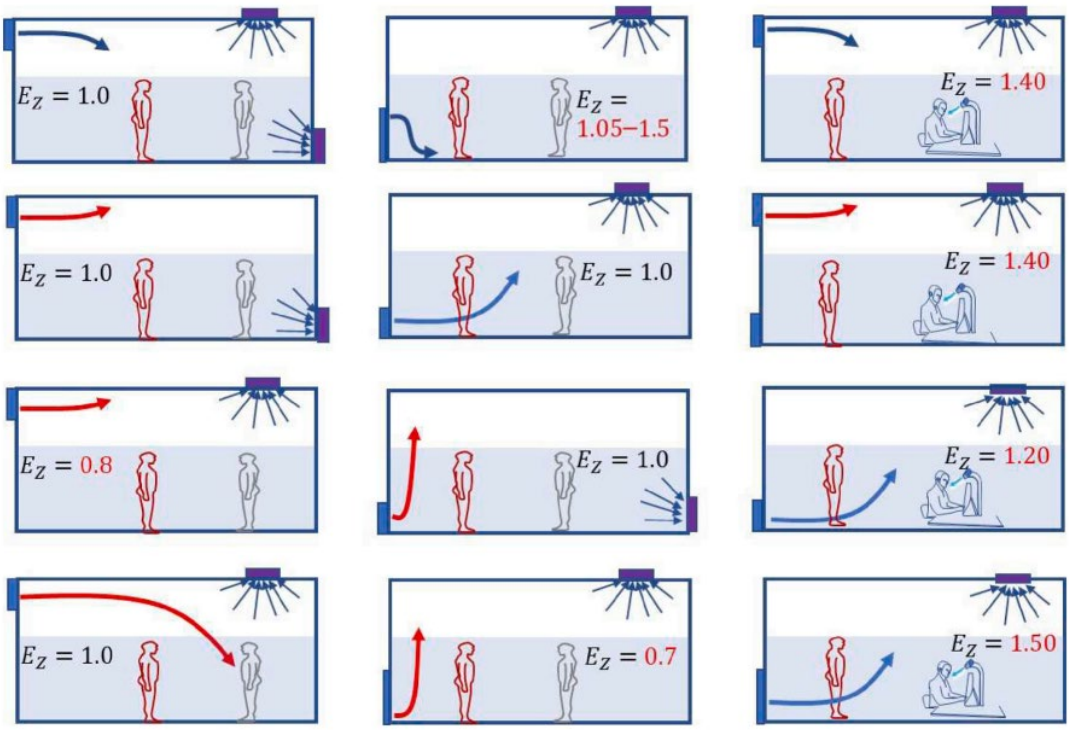

Figure 5

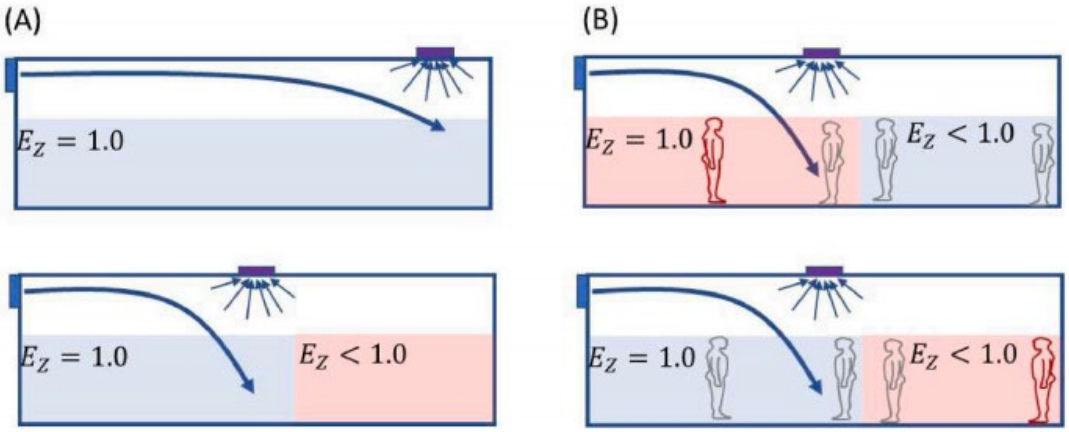

Figure 6

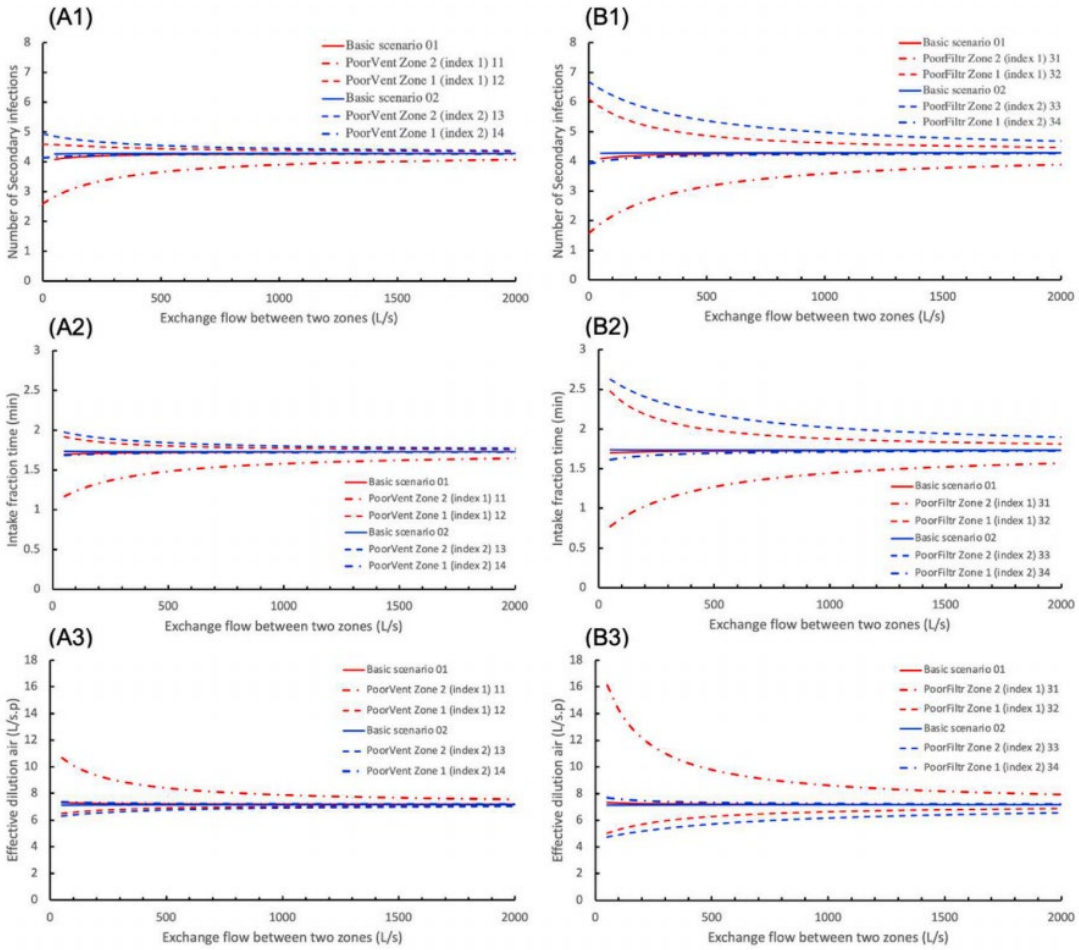
(A1)
Number of Secondary infections
Exchange flow between two zones (L/s)
Basic scenario 01
PoorVent Zone 2 (index 1) 11
PoorVent Zone 1 (index 1) 12
Basic scenario 02
PoorVent Zone 2 (index 2) 13
PoorVent Zone 1 (index 2) 14
(B1)
Number of Secondary infections
Exchange flow between two zones (L/s)
Basic scenario 01
PoorFiltr Zone 2 (index 1) 31
PoorFiltr Zone 1 (index 1) 32
Basic scenario 02
PoorFiltr Zone 2 (index 2) 33
PoorFiltr Zone 1 (index 2) 34
(A2)
Intake fraction time (min)
Exchange flow between two zones (L/s)
Basic scenario 01
PoorVent Zone 2 (index 1) 11
PoorVent Zone 1 (index 1) 12
Basic scenario 02
PoorVent Zone 2 (index 2) 13
PoorVent Zone 1 (index 2) 14
(B2)
Intake fraction time (min)
Exchange flow between two zones (L/s)
Basic scenario 01
PoorFiltr Zone 2 (index 1) 31
PoorFiltr Zone 1 (index 1) 32
Basic scenario 02
PoorFiltr Zone 2 (index 2) 33
PoorFiltr Zone 1 (index 2) 34
(A3)
Effective dilution air (L/s.p)
Exchange flow between two zones (L/s)
Basic scenario 01
PoorVent Zone 2 (index 1) 11
PoorVent Zone 1 (index 1) 12
Basic scenario 02
PoorVent Zone 2 (index 2) 13
PoorVent Zone 1 (index 2) 14
(B3)
Effective dilution air (L/s.p)
Exchange flow between two zones (L/s)
Basic scenario 01
PoorFiltr Zone 2 (index 1) 31
PoorFiltr Zone 1 (index 1) 32
Basic scenario 02
PoorFiltr Zone 2 (index 2) 33
PoorFiltr Zone 1 (index 2) 34

Figure 7

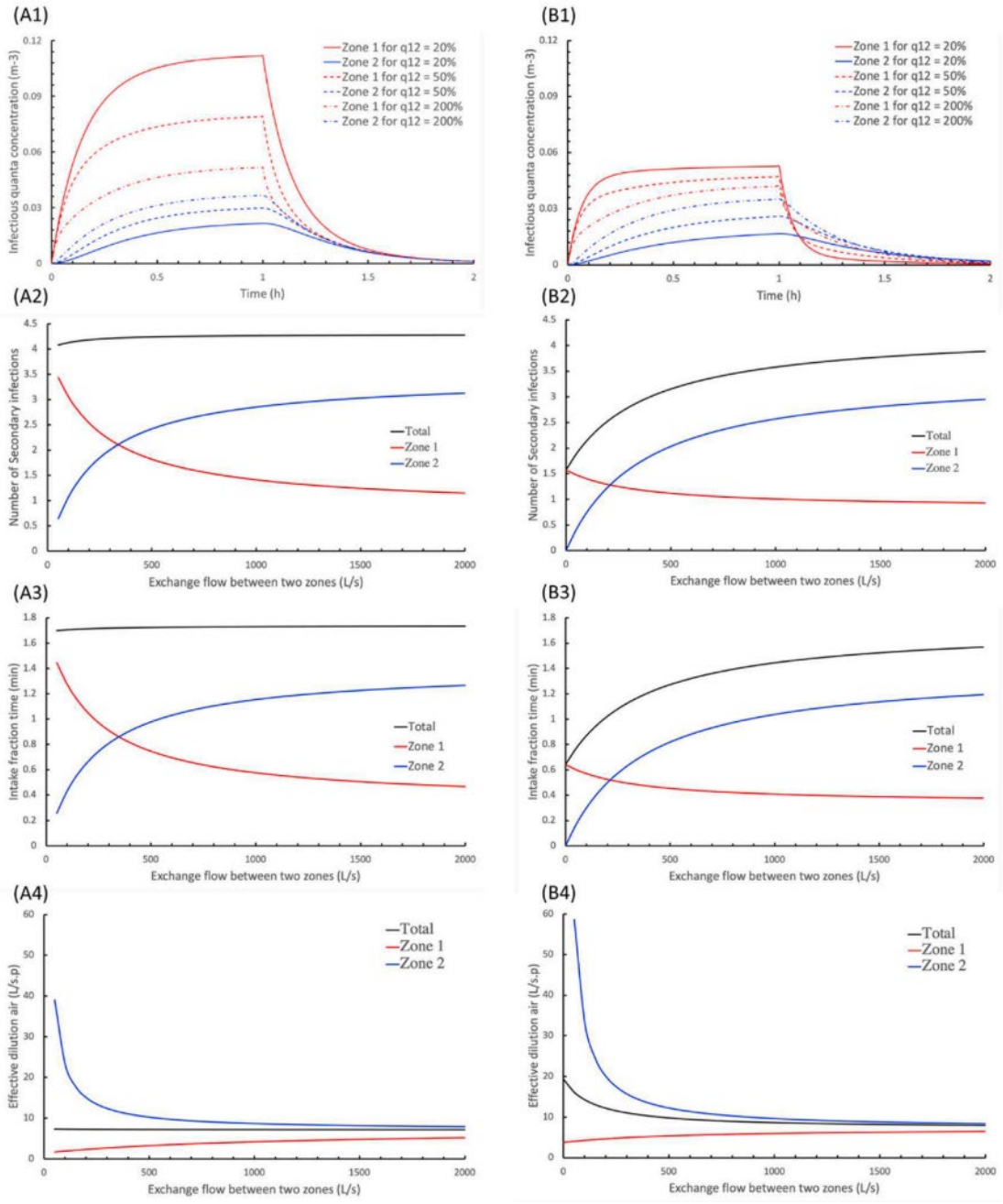
(A1)
Infectious quanta concentration (m-3)
Time (h)
Zone 1 for q12 = 20%
Zone 2 for q12 = 20%
Zone 1 for q12 = 50%
Zone 2 for q12 = 50%
Zone 1 for q12 = 200%
Zone 2 for q12 = 200%
(B1)
Infectious quanta concentration (m-3)
Time (h)
Zone 1 for q12 = 20%
Zone 2 for q12 = 20%
Zone 1 for q12 = 50%
Zone 2 for q12 = 50%
Zone 1 for q12 = 200%
Zone 2 for q12 = 200%
(A2)
Number of Secondary infections
Exchange flow between two zones (L/s)
Total
Zone 1
Zone 2
(B2)
Number of Secondary infections
Exchange flow between two zones (L/s)
Total
Zone 1
Zone 2
(A3)
Intake fraction time (min)
Exchange flow between two zones (L/s)
Total
Zone 1
Zone 2
(B3)
Intake fraction time (min)
Exchange flow between two zones (L/s)
Total
Zone 1
Zone 2
(A4)
Effective dilution air (L/s.p)
Exchange flow between two zones (L/s)
Total
Zone 1
Zone 2
(B4)
Effective dilution air (L/s.p)
Exchange flow between two zones (L/s)
Total
Zone 1
Zone 2

Figure 8

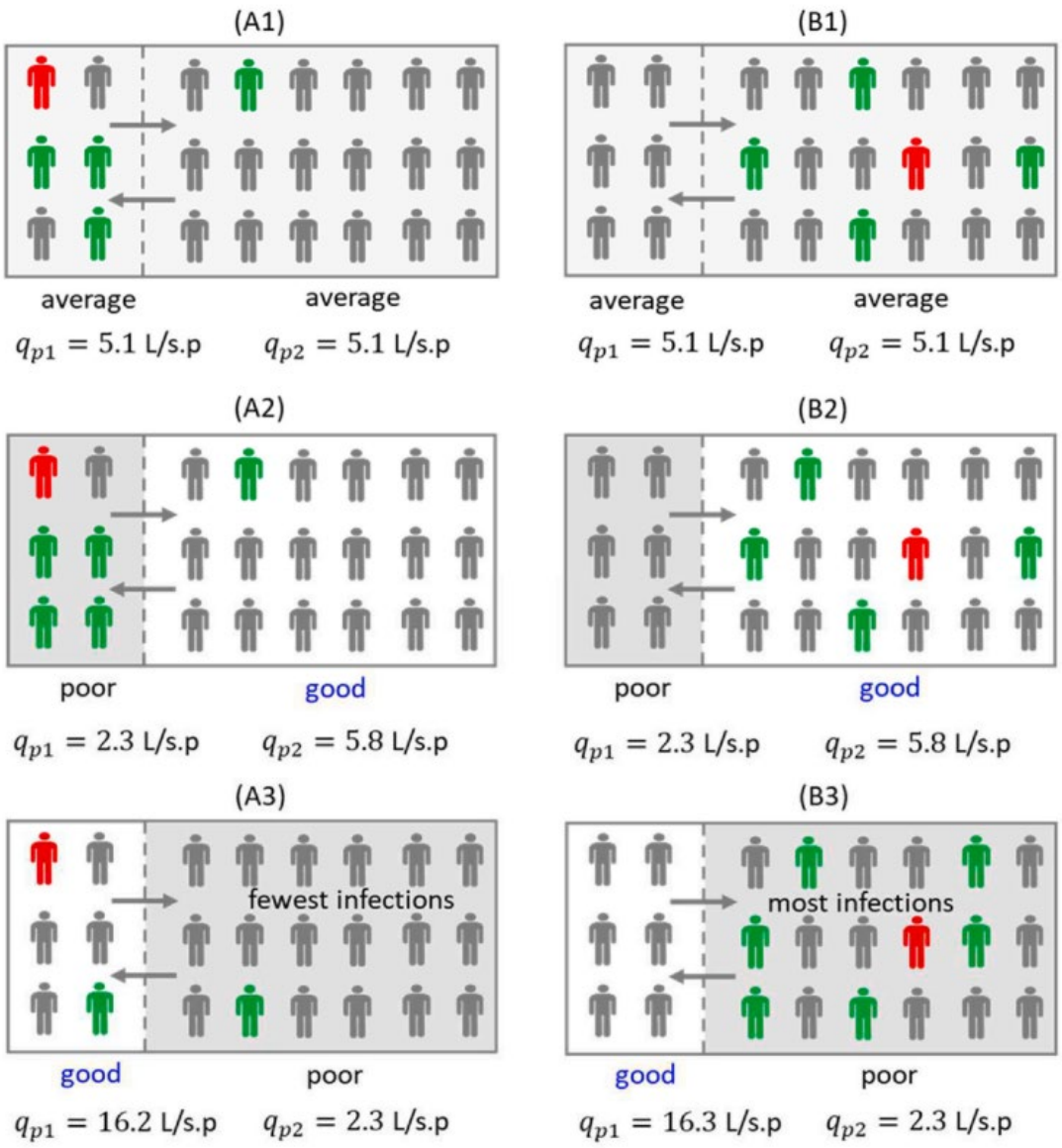
(A1)
average
average
$q_{p1} = 5.1$ L/s.p
$q_{p2} = 5.1$ L/s.p
(B1)
average
average
$q_{p1} = 5.1$ L/s.p
$q_{p2} = 5.1$ L/s.p
(A2)
poor
good
$q_{p1} = 2.3$ L/s.p
$q_{p2} = 5.8$ L/s.p
(B2)
poor
good
$q_{p1} = 2.3$ L/s.p
$q_{p2} = 5.8$ L/s.p
(A3)
fewest infections
good
poor
$q_{p1} = 16.2$ L/s.p
$q_{p2} = 2.3$ L/s.p
(B3)
most infections
good
poor
$q_{p1} = 16.3$ L/s.p
$q_{p2} = 2.3$ L/s.p

Table 1

The arrival time, $t_{1,i}$, and departure time, $t_{2,i}$, of patrons at each table.

Table	Arrival (24-h time)	Departure (24-h time)	Exposure starts at Table A (min)	Exposure ends (min)
A	12:01	13:23	0	82
B	11:37	12:54	0	53
C	12:03	13:18	2	77
04	na	na	na	na
05	11:32	12:53	0	52
06	11:36	13:23	0	82
07	11:29	13:10	0	69
08	12:28	13:37	27	96
09	11:47	13:16	0	75
10	11:07	13:28	0	87
11	11:32	13:11	0	70
12	12:13	13:17	12	76
13	11:53	12:51	0	50
14	11:23	13:02	0	61
15	11:55	13:30	0	89
16	11:24	12:49	0	48
17	13:00	14:19	59	138
18	11:34	13:18	0	77

Values in red indicate either arrival after the patrons at Table A arrived, or departure after the patrons at Table A departed. na, not applicable.

Table 2

The scenarios in the hypothetical two-zone restaurant.

Case number	Zone 1	Zone 2
01 [Zone 1, standard, standard] Basic scenario	$N_I = 1;\ N_o = 39, n_{o1} = 0.72, n_d = 0.67, n_s = 0.3, n_{f1} = 2;\ q_{p1} = 5.1$	$N_I = 0;\ N_o = 160, n_{o2} = 0.72, n_d = 0.67, n_s = 0.3, n_{f2} = 2;\ q_{p2} = 5.1$
02 [Zone 2, standard, standard] Basic scenario	$N_I = 0;\ N_o = 40, n_{o1} = 0.72, n_d = 0.67, n_s = 0.3, n_{f1} = 2;\ q_{p1} = 5.1$	$N_I = 1;\ N_o = 159, n_{o2} = 0.72, n_d = 0.67, n_s = 0.3, n_{f2} = 2;\ q_{p2} = 5.1$
11 [Zone 1, $n_{o1} = 3.6, n_{o2} = 0$] Poorly ventilated Zone 2 Index case in Zone 1	$N_I = 1;\ N_o = 39, n_{o1} = 3.6, n_d = 0.67, n_s = 0.3, n_{f1} = 2;\ q_{p1} = 9.1$	$N_I = 0;\ N_o = 160, n_{o2} = 0, n_d = 0.67, n_s = 0.3, n_{f2} = 2;\ q_{p2} = 4.1$
12 [Zone 1, $n_{o1} = 0, n_{o2} = 0.9$] Poorly ventilated Zone 1 Index case in Zone 1	$N_I = 1;\ N_o = 39, n_{o1} = 0, n_d = 0.67, n_s = 0.3, n_{f1} = 2;\ q_{p1} = 4.1$	$N_I = 0;\ N_o = 160, n_{o2} = 0.9, n_d = 0.67, n_s = 0.3, n_{f2} = 2;\ q_{p2} = 5.4$
13 [Zone 2, $n_{o1} = 3.6, n_{o2} = 0$] Poorly ventilated Zone 2 Index case in Zone 2	$N_I = 0;\ N_o = 40, n_{o1} = 3.6, n_d = 0.67, n_s = 0.3, n_{f1} = 2;\ q_{p1} = 9.1$	$N_I = 1;\ N_o = 159, n_{o2} = 0, n_d = 0.67, n_s = 0.3, n_{f2} = 2;\ q_{p2} = 4.1$
14 [Zone 2, $n_{o1} = 0, n_{o2} = 0.9$] Poorly ventilated Zone 1 Index case in Zone 2	$N_I = 0;\ N_o = 40, n_{o1} = 0, n_d = 0.67, n_s = 0.3, n_{f1} = 2;\ q_{p1} = 4.1$	$N_I = 1;\ N_o = 159, n_{o2} = 0.9, n_d = 0.67, n_s = 0.3, n_{f2} = 2;\ q_{p2} = 5.4$
31 [Zone 1, $n_{f1} = 10, n_{f2} = 0$] Poorly filtrated Zone 2 Index case in Zone 1	$N_I = 1;\ N_o = 39, n_{o1} = 0.72, n_d = 0.67, n_s = 0.3, n_{f1} = 10;\ q_{p1} = 16.2$	$N_I = 0;\ N_o = 160, n_{o2} = 0.72, n_d = 0.67, n_s = 0.3, n_{f2} = 0;\ q_{p2} = 2.3$
32 [Zone 1, $n_{f1} = 0, n_{f2} = 2.5$] Poorly filtrated Zone 1 Index case in Zone 1	$N_I = 1;\ N_o = 39, n_{o1} = 0.72, n_d = 0.67, n_s = 0.3, n_{f1} = 0;\ q_{p1} = 2.3$	$N_I = 0;\ N_o = 160, n_{o2} = 0.72, n_d = 0.67, n_s = 0.3, n_{f2} = 2.5;\ q_{p2} = 5.8$
33 [Zone 2, $n_{f1} = 10, n_{f2} = 0$] Poorly filtrated Zone 2 Index case in Zone 2	$N_I = 0;\ N_o = 40, n_{o1} = 0.72, n_d = 0.67, n_s = 0.3, n_{f1} = 10;\ q_{p1} = 16.2$	$N_I = 1;\ N_o = 159, n_{o2} = 0.72, n_d = 0.67, n_s = 0.3, n_{f2} = 0;\ q_{p2} = 2.3$
34 [Zone 2, $n_{f1} = 0, n_{f2} = 2.5$] Poorly filtrated Zone 1 Index case in Zone 2	$N_I = 0;\ N_o = 40, n_{o1} = 0.72, n_d = 0.67, n_s = 0.3, n_{f1} = 0;\ q_{p1} = 2.3$	$N_I = 1;\ N_o = 159, n_{o2} = 0.72, n_d = 0.67, n_s = 0.3, n_{f2} = 2.5;\ q_{p2} = 5.8$

Each case is presented as Case # [Index case zone, Zone 1 setting, Zone 2 setting]. The clean air flow rate per person in the entire restaurant remained unchanged at 5.1 L/s per person in all cases. The clean air flow rate per person in Zone 1, q_{p1}, and in Zone 2, q_{p2}, varied between cases. The index case was in either Zone 1 or Zone 2.

Table 3

Estimation of the infectious quantum emission rate when the zonal or total space is assumed to be fully mixed.

Parameters	Method					
	1	2	3	4	5	6
	1-Zone whole	1-Zone ABC	2-Zone whole	2-Zone ABC	2-Zone Individual + whole	2-Zone individual + ABC
No. of susceptible patrons	88	20	88	20 (68) †	88	20 (68) †
No. of secondary infections	9	9	9	9 (0) †	9	9 (0) †
Attack rate (%)	9/88, 10.2%	9/20, 45%	9/88, 10.2%	9/20, 45% (0/68, 0%) †	9/88, 10.2%	9/20, 45% (0/68, 0%) †
Exposure time (min)	Average 72.35	Average 73.75	Average 72.35	Average 73.75	Variable Table 1	
Air volume (m^3)	431	96	Zone 1: 96 Zone 2: 335			
$n_c = n + n_d + n_f + n_s$ (h^{-1})	5.66 = 0.67 + 0.63 + 0.30 + 4.06	4.83 = 0 + 0.63 + 0.3 + 3.9	Zone 1: 4.83 = 0 + 0.63 + 0.3 + 3.9 Zone 2: 5.89 = 0.86 + 0.63 + 0.3 + 4.1			
Quanta generation rate estimated (steady) (h^{-1})	132.2	136.7	127.7	333.4	127.4	335.7
Quanta generation rate estimated (transient) (h^{-1})	154.9[a]	164.3	150.6	369.0	152.1	368.8

(&) †, in which # and & refers to data of ABC and non-ABC zones, respectively, e.g., the number of secondary infections or attack rate.

[a] [12] provided an estimated quanta generation rate of 79.3 quanta/h using the transient Wells-Riley equation without considering the filtering effect of fan coil units, i.e., $n_f = 0$.